

International Journal of Modern Physics A
 © World Scientific Publishing Company

Status of rare exclusive B meson decays in 2018

Johannes Albrecht

*Fakultät Physik, Technische Universität Dortmund, Otto-Hahn-Straße 4a, 44227 Dortmund,
 Germany
 johannes.albrecht@tu-dortmund.de*

Stefanie Reichert

*Fakultät Physik, Technische Universität Dortmund, Otto-Hahn-Straße 4a, 44227 Dortmund,
 Germany
 stefanie.reichert@cern.ch*

Danny van Dyk*

*Physik Department, Technische Universität München, James-Frank-Straße 1, 85748 Garching,
 Germany
 danny.van.dyk@gmail.com*

Received Day Month Year
 Revised Day Month Year

This review discusses the present experimental and theoretical status of rare flavour-changing neutral current b -quark decays at the beginning of 2018. It includes a discussion of the experimental situation and details of the currently observed anomalies in measurements of flavour observables, including lepton flavour universality. Progress on the theory side, within and beyond the Standard Model theory is also discussed, together with potential New Physics interpretations of the present measurements.

Keywords: Flavour Physics, Rare Decays, Exclusive B Decays

PACS numbers: 13.20.He 13.30.Ce 12.15.Mm 12.60.Jv

Contents

1. Introduction	2
2. Anatomy of the amplitudes	3
3. Experimental measurements	6
3.1. Semileptonic $b \rightarrow s\ell^+\ell^-$ decays	6
3.1.1. $B \rightarrow K\ell^+\ell^-$ decays	6
3.1.2. $B \rightarrow K^*\ell^+\ell^-$ decays	9
3.1.3. $B \rightarrow K^*\ell^+\ell^-$ decays beyond the ground state	17

*TUM-HEP-1146/18

2 *Johannes Albrecht, Stefanie Reichert, Danny van Dyk*

3.1.4.	$B_s^0 \rightarrow \phi \ell^+ \ell^-$ decays	17
3.1.5.	Sum of exclusive $b \rightarrow s \ell^+ \ell^-$ decays	18
3.1.6.	$A_b^0 \rightarrow \Lambda \ell^+ \ell^-$ decays	20
3.1.7.	Tests of lepton flavour universality	21
3.2.	A note on $b \rightarrow d \ell^+ \ell^-$ decays	24
3.3.	Leptonic rare $B_{(s)}^0 \rightarrow \ell^+ \ell^-$ decays	25
3.4.	Exclusive $b \rightarrow s \gamma$ decays	28
4.	Theory of rare $b \rightarrow s \ell^+ \ell^-$ decays	29
4.1.	Hadronic matrix elements of local operators	29
4.2.	Hadronic matrix elements of non-local operators	31
4.3.	Theory predictions in the Standard Model	34
5.	Phenomenology and New Physics reach	35
5.1.	Global fits	35
6.	Experimental outlook	37

1. Introduction

The year 2018 marks a special point for the field of particle physics as it is not only the end of second period of data-taking at the Large Hadron Collider(LHC) but also the start-up of the Belle II experiment. In the field of flavour physics, a number of anomalies have been observed when comparing measurements to the Standard Model (Standard Model (SM)) expectation; from which a coherent and conclusive picture emerges. Those anomalies could, if they persist, point towards certain New Physics (NP) models such as leptoquarks or Z' bosons. In this review, we will give a comprehensive overview of the current state-of-the-art of exclusive rare b decays from both experimental and theoretical perspective. We will present the current experimental landscape with a focus of the observed anomalies and discuss potential new physics interpretations.

The LHCb experiment will continue to run for the next two decades and hence will be able to either confirm or rule out many of the present-day anomalies. With the imminent start-up of the data-taking at the Belle II experiment, these tensions will be independently cross-checked and further complementary measurements will be accessible.

As the progress in inclusive $b \rightarrow s \ell^+ \ell^-$ decays was limited after the end of the B factories, this review focusses on exclusive measurements of rare decays of B hadrons as these are excellent probes for many new physics scenarios. These rare decay processes are CKM-, GIM- and loop-suppressed, wherefore potential new physics effects can be large compared to the SM amplitude. Such indirect searches allow to probe NP models at much higher mass scales as are currently accessible through direct searches. In the past, exclusive decays with muons in the final state have been measured extensively by the LHC experiments, most notably by LHCb, as well as the B factories. We review the status of these measurements, discuss their theoretical description in the SM and model-independently in the presence of

new physics. A special focus is set on the anomalies seen in angular distributions of $B^0 \rightarrow K^{*0} \mu^+ \mu^-$ and in the branching fraction measurements of all exclusive $b \rightarrow s \ell^+ \ell^-$ decays as well as to the tensions observed in tests of lepton flavour universality in this class of decays. Measurements of the type $b \rightarrow c \ell \nu$ are not covered in this review.

On the theoretical side, the current state of the SM predictions for the discussed observables is presented. The anatomy of the amplitudes, and their dependence on various local and non-local hadronic matrix elements is discussed. Particular focus is set on recent developments for the non-local matrix elements. The model-independent interpretation of the $b \rightarrow s \ell^+ \ell^-$ measurements is examined in the framework of the usual Effective Field Theory.

This review is structured as follows: Section 2 introduces the amplitudes of $b \rightarrow s \ell^+ \ell^-$ decays in an effective field theory approach. Section 3 discusses the experimental landscape with a focus on semileptonic $b \rightarrow s \ell^+ \ell^-$ decays, which is followed by a brief discussion of $b \rightarrow d \ell^+ \ell^-$ decays, purely leptonic $B_{(s)}^0 \rightarrow \ell^+ \ell^-$ and $b \rightarrow s \gamma$ decays. The experimental part of the review closes with a brief discussion of $b \rightarrow s \gamma$ decays.

The second part of the review, Section 4, examines the foundation for the SM predictions required in the first part of the review. Section 5 discusses then a combined interpretation of all presented measurements in the framework of global fits and possible interpretations of the observed patterns in NP frameworks.

The review closes with a discussion of the experimental outlook in Section 6.

2. Anatomy of the amplitudes

Within the SM and at the Born level there are no flavor-changing neutral currents (FCNC). As a consequence, any FCNC-mediated quark-flavor transitions, such as $b \rightarrow s$, emerge only from virtual loop corrections, in which a W is first emitted and subsequently re-absorbed. The emergence at the loop level naturally suppresses the rate at which these processes occur. In the SM, the unitarity of the Cabibbo-Kobayashi-Maskawa (CKM) matrix introduces an additional suppression mechanism that renders $b \rightarrow s \ell^+ \ell^-$ transitions *very rare*.¹ Moreover, descriptions of these rare b decays in the SM are further complicated since they pose a multi-scale problem: as weak decays they are mediated through the exchange of W and Z bosons, which are much heavier than the remaining particles (with the exception of the t quark). The use of an Effective Field Theory (EFT) helps our understanding of such multi-scale dynamics. In the following, we will discuss the EFT used for predictions of rare b decays below the electroweak breaking scale $\Lambda_{\text{EW}} \simeq 80 \text{ GeV}$. Within the SM, this EFT captures the effects of the t quark as well as the W and Z bosons, which are no-longer dynamical degrees of freedom for scales $\mu < \Lambda_{\text{EW}}$.

The effective Lagrangian reads (see *e.g.*¹)

$$\mathcal{L}_{b \rightarrow s \ell^+ \ell^-} = \mathcal{L}_{\text{QED}} + \mathcal{L}_{\text{QCD},5} + \frac{4G_{\text{F}}}{\sqrt{2}} V_{tb} V_{ts}^* \left[\sum_i C_i(\mu) O_i \right] + \mathcal{O}(V_{ub} V_{us}^*), \quad (1)$$

4 Johannes Albrecht, Stefanie Reichert, Danny van Dyk

where \mathcal{L}_{QED} and $\mathcal{L}_{\text{QCD},5}$ denote the Lagrangians of the electromagnetic and strong interactions (with five quark flavours after integrating out the top quark), G_F refers to the Fermi constant, and the last term captures the local effective operators O_i with their effective couplings - or Wilson coefficients (WC)- C_i at the renormalisation scale μ . For convenience, the product of CKM matrix elements $V_{tb}V_{ts}^*$ has been extracted from the definition of the WC.

The matrix elements of the effective operators O_i need to be evaluated at a low scale $\mu_b = m_b \simeq 4.2 \text{ GeV}$, which minimises logarithms in the perturbative expansion of the matrix elements. Consequently, one requires the WC evaluated at μ_b . Problems arising from large logarithms $\ln(M_W/\mu_b)$ are resummed through Renormalisation Group (RG) improved running. Contemporary analyses use resummation of QCD-induced large logarithms up to Next-to-Next-to-Leading-Logarithm (NNLL). This requires knowledge of the relevant anomalous dimensions at the four-loop level, and the matching conditions at the three-loop level.²⁻⁶ The electroweak effects to NLL, which are numerically sub-leading, are known only for a subset of the WC.⁷

For a consistent treatment at the leading order in the electromagnetic coupling e , all operators of the following set - usually called the SM basis - are required (see *e.g.*²). The SM basis consists of the current-current operators ($q = u, c$)

$$O_{1q} = [\bar{s}\gamma^\mu T^A P_L q] [\bar{q}\gamma_\mu T^A P_L b], \quad O_{2q} = [\bar{s}\gamma^\mu P_L q] [\bar{q}\gamma_\mu P_L b]; \quad (2)$$

the QCD-penguin operators

$$\begin{aligned} O_3 &= [\bar{s}\gamma^\mu P_L b] \sum_q [\bar{q}\gamma_\mu q], & O_4 &= [\bar{s}\gamma^\mu T^A P_L b] \sum_q [\bar{q}\gamma_\mu T^A q], \\ O_5 &= [\bar{s}\gamma^{\mu\nu\rho} P_L b] \sum_q [\bar{q}\gamma_{\mu\nu\rho} q], & O_6 &= [\bar{s}\gamma^{\mu\nu\rho} T^A P_L b] \sum_q [\bar{q}\gamma_{\mu\nu\rho} T^A q]; \end{aligned} \quad (3)$$

the electromagnetic and chromomagnetic dipole operators

$$O_7 = \frac{e}{16\pi^2} \bar{m}_b [\bar{s}\sigma^{\mu\nu} P_R b] F_{\mu\nu}, \quad O_8 = \frac{g_s}{16\pi^2} \bar{m}_b [\bar{s}\sigma^{\mu\nu} T^A P_R b] G_{\mu\nu}^A; \quad (4)$$

and the semileptonic operators

$$O_9 = \frac{e^2}{16\pi^2} [\bar{s}\gamma^\mu P_L b] [\bar{\ell}\gamma_\mu \ell], \quad O_{10} = \frac{e^2}{16\pi^2} [\bar{s}\gamma^\mu P_L b] [\bar{\ell}\gamma_\mu \gamma_5 \ell]. \quad (5)$$

In the above, we abbreviate $\gamma^{\mu\nu\rho} \equiv \gamma^\mu \gamma^\nu \gamma^\rho$, $P_{L(R)} \equiv (1 \mp \gamma_5)/2$, $e^2 = 4\pi\alpha_e$, and sums over q run over all active quark flavours u, d, s, c , and b . Through using $\alpha_e = \alpha_e(\mu_b)$, universal QED corrections at NLO are taken care of.^{8,9}

Searches for NP effects at energies smaller than $\mu \approx M_W$ have so far not discovered either new interactions or new particles. Assuming that no such low-mass fields exist, the EFT framework, which is necessary for accurate theory predictions, can also be used to systematically describe NP effects. To this end, the effective Lagrangian Eq. (1) has to be modified in the following way:¹⁰

- (1) the set of effective field operators is enlarged to include all operators allowed by field content and Lorentz symmetry up to a given mass dimension (typically mass dimension six),
- (2) their WC are assumed to be independent and uncorrelated parameters.

When limiting this enlarged set to only semileptonic operators, a basis of all operators up to and including mass dimension six can be formed by also including the chirality-flipped operators,

$$O_{9'} = \frac{e^2}{16\pi^2} [\bar{s}\gamma^\mu P_R b] [\bar{\ell}\gamma_\mu \ell], \quad O_{10'} = \frac{e^2}{16\pi^2} [\bar{s}\gamma^\mu P_R b] [\bar{\ell}\gamma_\mu \gamma_5 \ell]; \quad (6)$$

the (pseudo)scalar operators

$$\begin{aligned} O_S &= \frac{e^2}{16\pi^2} [\bar{s}\gamma^\mu P_R b] [\bar{\ell}\ell], & O_P &= \frac{e^2}{16\pi^2} [\bar{s}\gamma^\mu P_R b] [\bar{\ell}\gamma_5 \ell], \\ O_{S'} &= \frac{e^2}{16\pi^2} [\bar{s}\gamma^\mu P_L b] [\bar{\ell}\ell], & O_{P'} &= \frac{e^2}{16\pi^2} [\bar{s}\gamma^\mu P_L b] [\bar{\ell}\gamma_5 \ell]; \end{aligned} \quad (7)$$

and the tensor operators

$$O_T = \frac{e^2}{16\pi^2} [\bar{s}\sigma^{\mu\nu} b] [\bar{\ell}\sigma_{\mu\nu} \ell], \quad O_{T5} = \frac{e^2}{16\pi^2} [\bar{s}\sigma^{\mu\nu} b] [\bar{\ell}\sigma_{\mu\nu} \gamma_5 \ell]. \quad (8)$$

A complete and non-redundant set of dimension-six operators, including their one-loop anomalous dimensions in both QCD and QED is compiled in.¹¹

This *bottom up* approach probes model-independently for deviations from the SM:^{12–15} the WCs are sensitive to NP effects of new particles that are too heavy to be produced directly. Rare semileptonic b decays therefore provide information that is complementary to the “direct” searches for new interactions and particles that are carried out at the Large Hadron Collider.

The above basis is further reduced when one assumes a manifest invariance of NP effects under the SM gauge group within a SM-like (i.e. linear σ) Higgs model. For the $b \rightarrow s\ell^+\ell^-$ operators, this was explicitly demonstrated in.^{16a} The effective Lagrangian in Eq. (1) can be matched onto the SM Effective Field Theory (SMEFT) (see *e.g.*¹⁸), whose operators are manifestly invariant under the SM gauge group. The required matching formulas are compiled in¹⁹ to leading non-trivial loop level. Matching, basis transformations and Renormalization-Group-Equation (RGE) evolution can be conveniently achieved through a variety of computational tools, including but not limited to: the “DsixTools” Mathematica package;²⁰ the “Wilson Coefficient Exchange Format” and its reference Python implementation;²¹ and the “Wilson” Python package.²²

^a Note, however, that a nonlinear representation fully restores the basis of dimension six operators to the set introduced above.¹⁷

6 Johannes Albrecht, Stefanie Reichert, Danny van Dyk

Schematically, the matrix elements for all exclusive $b \rightarrow s\ell^+\ell^-$ processes can now be expressed as

$$\mathcal{A} \sim C_{10}\mathcal{F}_{10} + \left[C_9\mathcal{F}_9 - \frac{2m_b M_B}{q^2} C_7\mathcal{F}_7 \right] - \frac{32\pi^2 M_B^2}{q^2} \mathcal{H} + \mathcal{O}(\alpha_e), \quad (9)$$

where q^2 refers to the invariant mass squared of the di-lepton pair. The \mathcal{F}_i refer to hadronic matrix elements of local $\bar{s}b$ currents as induced by the operators $O_{7,9,10}$, while \mathcal{H} denotes matrix elements of time-ordered products involving four-quark operators $O_{1c,2c,3,\dots,6}$ and the chromomagnetic operator O_8 together with the electromagnetic current. In the presence of NP effects in the semileptonic and radiative operators, the hadronic matrix elements remain unchanged. However, the coefficients multiplying the latter are then modified. For the complete anatomy of the amplitudes of $B \rightarrow K^{(*)}\ell^+\ell^-$ decays in the presence of NP operators of mass dimension six we refer to.^{23,24} A similar study for $A_b^0 \rightarrow A\ell^+\ell^-$ is presented in.²⁵

3. Experimental measurements

In this section, we draw a picture of the current experimental status of semi-leptonic $b \rightarrow s\ell^+\ell^-$ (including a brief discussion of $b \rightarrow d\ell^+\ell^-$) decays, purely leptonic $B_{(s)}^0 \rightarrow \ell^+\ell^-$ and radiative $b \rightarrow s\gamma$ transitions. Hereby, we will discuss measurements of the various hadronic final states, *e.g.* kaon and K^* states, giving access to a broad range of observables such as branching fractions, CP and isospin asymmetries as well as angular observables. Within this section, the LHCb measurements refer to the full Run 1 dataset corresponding to 3fb^{-1} collected during the years 2011 and 2012, the BaBar results were obtained on their full dataset of 424fb^{-1} and the Belle publications exploit their complete dataset of 711fb^{-1} if not otherwise stated. Presented results integrated over the whole q^2 range have been obtained by vetoing the charmonium resonances and interpolating over this vetoed q^2 region. It should be noted that the exact range to veto the charmonium resonances depends on the respective analysis.

3.1. Semileptonic $b \rightarrow s\ell^+\ell^-$ decays

Particular interest was raised throughout the past years by various measurements of semileptonic $b \rightarrow s\ell^+\ell^-$ decays, in which several tensions between the SM predictions and experimental measurements have been observed. These deviations are mostly in the range of two to three standard deviations and show a consistent pattern, which can be explained by lowering the WC C_9 with respect to its SM value^{14,26,27} as detailed further in Section 5.1.

3.1.1. $B \rightarrow K\ell^+\ell^-$ decays

The differential branching fractions of the decays $B^+ \rightarrow K^+\mu^+\mu^-$ and $B^0 \rightarrow K^0\mu^+\mu^-$ versus the invariant mass squared of the dimuon pair, q^2 , were determined by the LHCb collaboration with the CP -averaged isospin asymmetry A_1 ²⁸

defined as

$$A_I = \frac{\Gamma(B^0 \rightarrow K^{(*)0} \mu^+ \mu^-) - \Gamma(B^+ \rightarrow K^{(*)+} \mu^+ \mu^-)}{\Gamma(B^0 \rightarrow K^{(*)0} \mu^+ \mu^-) + \Gamma(B^+ \rightarrow K^{(*)+} \mu^+ \mu^-)}, \quad (10)$$

$$= \frac{\mathcal{B}(B^0 \rightarrow K^{(*)0} \mu^+ \mu^-) - (\tau_0/\tau_+) \cdot \mathcal{B}(B^+ \rightarrow K^{(*)+} \mu^+ \mu^-)}{\mathcal{B}(B^0 \rightarrow K^{(*)0} \mu^+ \mu^-) + (\tau_0/\tau_+) \cdot \mathcal{B}(B^+ \rightarrow K^{(*)+} \mu^+ \mu^-)}, \quad (11)$$

with the partial widths Γ and branching fractions \mathcal{B} of the corresponding decay channels and the ratio of B^0 to B^+ lifetimes τ_0/τ_+ . The analysis finds values individually compatible with the SM prediction. However, the entirety of measurements lies systematically below the predictions as shown in Fig. 1. In the same analysis, the CP -averaged isospin asymmetry has been measured and is depicted in Fig. 1. In a similar analysis, the CP asymmetry

$$\mathcal{A}_{CP} = \frac{\Gamma(\bar{B} \rightarrow \bar{K}^{(*)} \mu^+ \mu^-) - \Gamma(\bar{B} \rightarrow \bar{K}^{(*)} \mu^+ \mu^-)}{\Gamma(\bar{B} \rightarrow \bar{K}^{(*)} \mu^+ \mu^-) + \Gamma(\bar{B} \rightarrow \bar{K}^{(*)} \mu^+ \mu^-)}, \quad (12)$$

was determined under the assumption of no direct CP violation in the control mode $B^+ \rightarrow K^+ J/\psi$ to be $\mathcal{A}_{CP}(B^+ \rightarrow K^+ \mu^+ \mu^-) = 0.012 \pm 0.017 \pm 0.001$, where the uncertainties are statistical and systematic, respectively,²⁹ and this measurement is consistent with the SM prediction.³⁰

The double differential decay rate of $B^+ \rightarrow K^+ \mu^+ \mu^-$ decays³² is given by

$$\frac{1}{\Gamma} \frac{d\Gamma}{d \cos \theta_l} = \frac{3}{4}(1 - F_H)(1 - \cos^2 \theta_l) + \frac{1}{2}F_H + A_{FB} \cos \theta_l, \quad (13)$$

where the angle between the μ^- (μ^+) and the oppositely charged kaon K^+ (K^-) of the B^+ (B^-) decay is denoted by θ_l , F_H is the so-called flat term, and A_{FB} is the forward-backward asymmetry of the dimuon system.

As the flavour of the neutral B meson cannot be determined for the self-conjugate final state $K_s^0 \mu^+ \mu^-$, the double differential decay rate is extracted as a function of the absolute value of $\cos \theta_l$ as

$$\frac{1}{\Gamma} \frac{d\Gamma}{d |\cos \theta_l|} = \frac{3}{2}(1 - F_H)(1 - |\cos \theta_l|^2) + F_H, \quad (14)$$

with the constraint of $0 \leq F_H \leq 3$ enforcing the expression to be positive-definite for all values of $|\cos \theta_l|$.³³ The results of A_{FB} and F_H are compatible with the SM predictions³¹ and are shown in Fig. 2.

Interference effects between the short- and long-distance contributions were studied in $B^+ \rightarrow K^+ \mu^+ \mu^-$ decays at low recoil.³⁴ The LHCb collaboration reported the first observation of the decays $B^+ \rightarrow \Psi(4160)K^+$ and the subsequent decay $\Psi(4160) \rightarrow \mu^+ \mu^-$ with $\mathcal{B}(B^+ \rightarrow \Psi(4160)K^+) = (5.1_{-1.2}^{+1.3} \pm 3.0) \cdot 10^{-4}$, which is determined under the assumption of lepton flavour universality and hence the second uncertainty stems from the known $\Psi(4160) \rightarrow e^+ e^-$ branching fraction. No significant signal was observed for the $\Psi(4040)$ resonance, and an upper limit $\mathcal{B}(B^+ \rightarrow$

8 Johannes Albrecht, Stefanie Reichert, Danny van Dyk

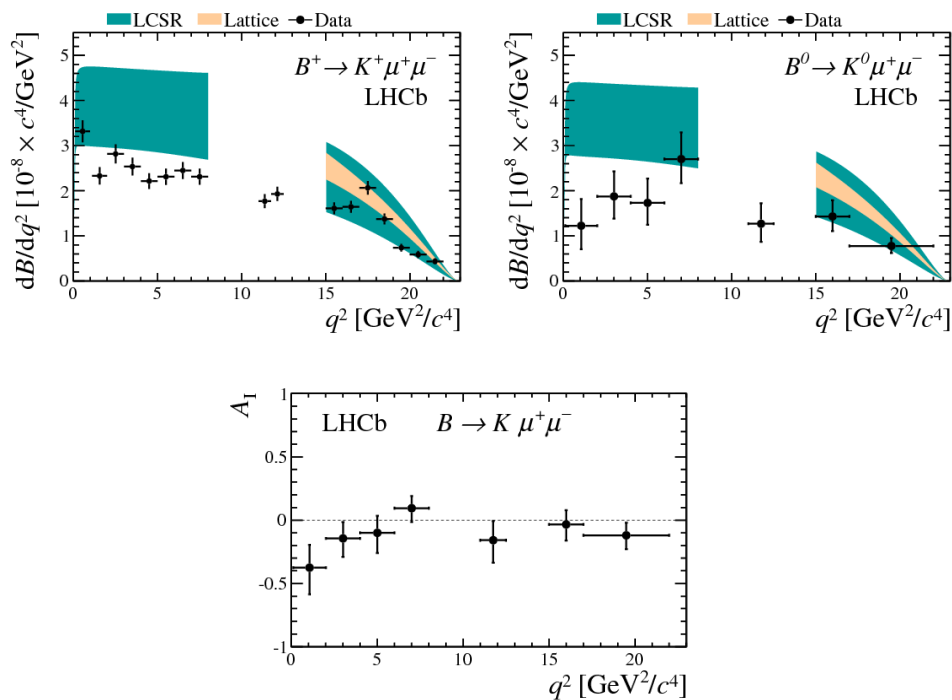


Fig. 1. Differential branching fraction results for $B^+ \rightarrow K^+ \mu^+ \mu^-$ (top left) and $B^0 \rightarrow K^0 \mu^+ \mu^-$ (top right) decays with theory predictions overlaid³¹ and the CP -averaged isospin asymmetry (bottom). Figures from²⁸

$\Psi(4040)K^+$) $< 1.3 (1.7) \cdot 10^{-4}$ at 90 (95)% C.L. is set. The mean and the width of the $\Psi(4160)$ resonance were measured to be $4191_{-8}^{+9} \text{ MeV}/c^2$ and $65_{-16}^{+22} \text{ MeV}/c^2$, respectively, where the uncertainties comprise both statistical and systematic sources. The interference between the observed resonant $B^+ \rightarrow \Psi(4160)K^+$ and the non-resonant $B^+ \rightarrow K^+ \mu^+ \mu^-$ decay in the large q^2 region amounts to 20%³⁴ leading to renewed interest in previous estimates of quark-hadron duality violation for these processes³⁵ as discussed in Section 4.2.

By assuming a model of hadronic resonances, the LHCb collaboration fits the differential branching fraction of $B^+ \rightarrow K^+ \mu^+ \mu^-$ to data. The branching fraction of the short-distance component is determined by setting the J/ψ and $\psi(2S)$ resonance amplitudes to zero, and is found to be $\mathcal{B}(B^+ \rightarrow K^+ \mu^+ \mu^-) = (4.37 \pm 0.15 \pm 0.23) \cdot 10^{-7}$,³⁶ where the uncertainties are statistical (including the form factor uncertainties) and systematic. In addition, the phase difference between the short-distance and the narrow-resonance amplitudes in $B^+ \rightarrow K^+ \mu^+ \mu^-$ decays was determined by performing a fit to the mass of the dimuon pair; of which one possible solution is illustrated in Fig. 3. As the values of the J/ψ phases are compatible with $\pm\pi/2$, the interference with the short-distance contributions far from

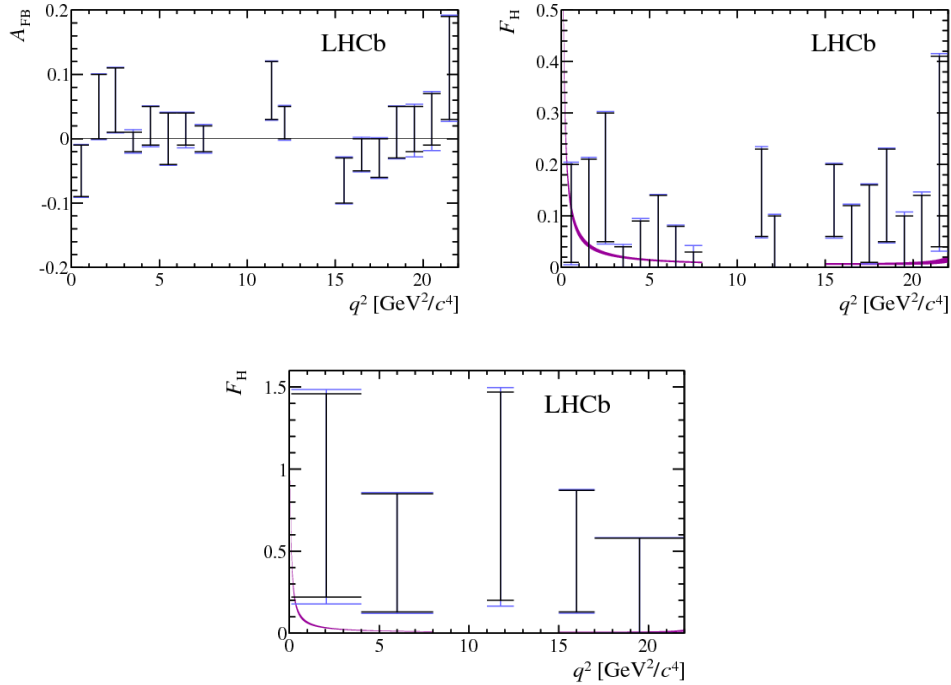


Fig. 2. Results for A_{FB} (left) and F_{H} in $B^+ \rightarrow K^+ \mu^+ \mu^-$ decays and for F_{H} in $B^0 \rightarrow K_{\text{S}}^0 \mu^+ \mu^-$ decays (bottom). The inner horizontal bars indicate the one-dimensional 68% confidence intervals, whereas the outer vertical bars include contributions from systematic uncertainties. The SM predictions are overlaid as band. Figures from.³³

the pole masses is small.

3.1.2. $B \rightarrow K^* \ell^+ \ell^-$ decays

In addition to the aforementioned studies of K^0 and K^+ states, channels with a pair of $K^+ \pi^-$ mesons in the final state have received particular attention over the past years as those decays show a rich phenomenology. Amongst these decays, events with a $K^+ \pi^-$ invariant mass close to the vector resonance K^* (892) are the subject of numerous studies. Here and in the following, we discuss treating the K^* (892) as a quasi-stable particle, and decays $B^0 \rightarrow K^{*0} \mu^+ \mu^-$ should be interpreted as the decay chain $B \rightarrow K^*(892)(\rightarrow K\pi) \mu^+ \mu^-$ if not otherwise stated.

The CP asymmetry defined in Eq. (12) was measured by the LHCb collaboration to be $\mathcal{A}_{CP}(B^0 \rightarrow K^{*0} \mu^+ \mu^-) = -0.035 \pm 0.024 \pm 0.003$, where the uncertainties are statistical and systematic, respectively,²⁹ and the measurement is found to be consistent with the SM expectation of a small CP asymmetry in this decay.

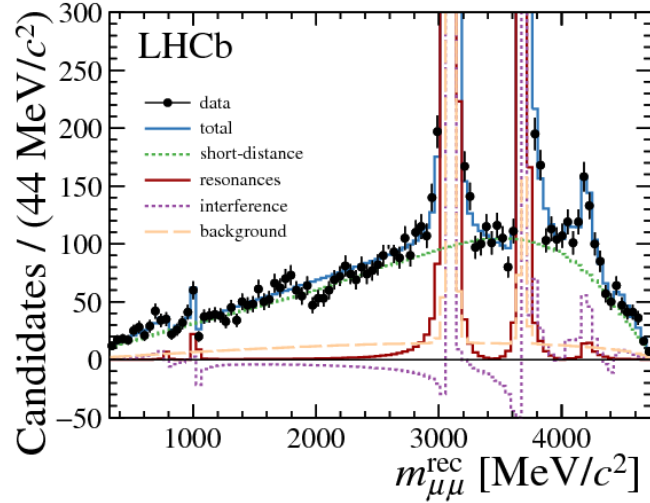


Fig. 3. Fit to the mass of the dimuon pair for the favoured case where both J/ψ and $\psi(2S)$ phases are negative. Figure from.³⁶

The differential branching fraction of a charged B meson into a K^{*+} final state, $B^+ \rightarrow K^{*+}\mu^+\mu^-$, has been measured by the LHCb collaboration; the results are shown in Fig. 4 in several bins of q^2 . A study of the neutral decay mode was performed, which resulted in the measurement of the isospin asymmetry as defined in Eq. (10) illustrated in Fig. 4. As the differential branching fractions of the decay $B^0 \rightarrow K^{*0}\mu^+\mu^-$ had been previously reported in,³⁷ the values were not updated in²⁸ until later in.³⁸ The latter results are as well depicted in Fig. 5, and the analysis yields the most precise measurement to date of the q^2 -averaged branching ratio

$$\mathcal{B}(B^0 \rightarrow K^{*0}\mu^+\mu^-)/\delta q^2 = (0.342_{-0.17}^{+0.17} \pm 0.009 \pm 0.023) \cdot 10^{-7} \frac{c^4}{\text{GeV}^2}, \quad (15)$$

with $\delta q^2 = 4.9 \text{ GeV}^2/c^4$ (in the bin $1.1 \text{ GeV}^2/c^4 < q^2 < 6.0 \text{ GeV}^2/c^4$) where the uncertainties are statistical, systematic and from the uncertainty on the branching fraction of the normalisation channel $B^0 \rightarrow K^{*0}J/\psi$. In the region $1.1 \text{ GeV}^2/c^4 < q^2 < 6.0 \text{ GeV}^2/c^4$ and for the $K^+\pi^-$ invariant mass range $796 \text{ MeV}/c^2 < m(K\pi) < 996 \text{ MeV}/c^2$, the S-wave component is measured to be $F_S = 0.101 \pm 0.017 \pm 0.009$,³⁸ where the uncertainties are of statistical and systematic origin. Assuming the absence of high-order waves *e.g.* D- and F-waves, the pure P-wave component of the differential branching fraction has been determined for the first time. However, in previous analyses, the S-wave fraction was not taken into account as is the case in a measurement of the differential branching fraction published by the CMS collaboration,³⁹ whose results are shown in Fig. 5.

The four-dimensional differential decay rate of $B^0 \rightarrow K^{*0}\mu^+\mu^-$ ($\bar{B}^0 \rightarrow \bar{K}^{*0}\mu^+\mu^-$) decays is expressed as a function of the invariant mass of the lepton

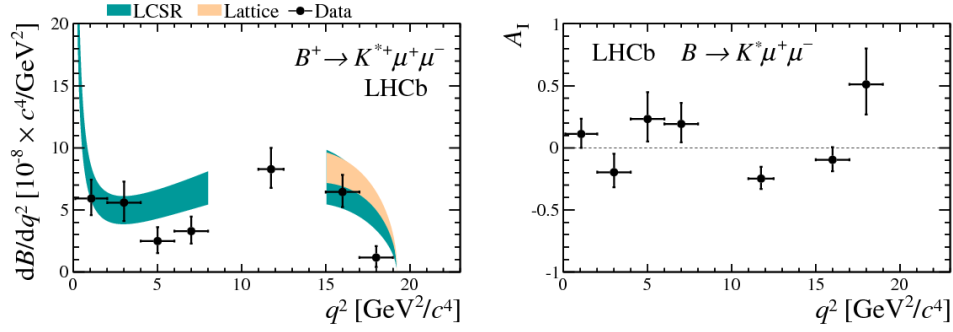


Fig. 4. Differential branching fraction results for $B^+ \rightarrow K^{*+} \mu^+ \mu^-$ (left) decays with theory predictions overlaid^{31,40} and the CP -averaged isospin asymmetry (right). Figures from.²⁸

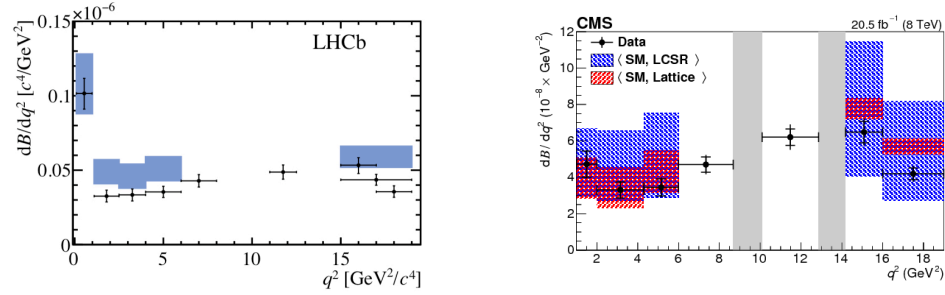


Fig. 5. Differential branching fraction results for the P-wave component of $B^0 \rightarrow K^{*0} \mu^+ \mu^-$ decays with theory predictions overlaid,^{41,42} which are purely made for the resonant P-wave part of the $K^+ \pi^-$ system (left)³⁸ and for the S- and P-wave components (right).³⁹

pair q , and the angles θ_ℓ , θ_{K^*} and ϕ , where θ_ℓ refers to the angle between the μ^- and the K^{*0} (\bar{K}^{*0}) flight directions in the di-lepton rest frame, and θ_{K^*} to the angle between the K^{*0} (\bar{K}^{*0}) and the K^+ (K^-) flight directions in the K^* rest frame and ϕ corresponds to the angle between the planes defined by the di-muon and the kaon and pion in the B rest frame.^{43,44} The fully differential decay rate is then given by

$$\frac{d^4\bar{\Gamma}(B^0 \rightarrow K^{*0} \mu^+ \mu^-)}{dq d\cos\theta_\ell d\cos\theta_{K^*} d\cos\phi} = \frac{9}{32\pi} \sum \bar{I}_i(q, \theta_{K^*}) f_i(\theta_\ell, \phi), \quad (16)$$

$$\frac{d^4\Gamma(\bar{B}^0 \rightarrow \bar{K}^{*0} \mu^+ \mu^-)}{dq d\cos\theta_\ell d\cos\theta_{K^*} d\cos\phi} = \frac{9}{32\pi} \sum I_i(q, \theta_{K^*}) f_i(\theta_\ell, \phi), \quad (17)$$

where the I_i (\bar{I}_i) terms depend on products of the K^* spin amplitudes and the f_i functions are the corresponding angular distribution functions^b assuming an on-shell K^* meson.³⁰ As the theoretical calculations define θ_ℓ with respect to the negatively

^bThe differential decay rate taking the full basis including scalar and tensor operators has been derived in.²³

12 Johannes Albrecht, Stefanie Reichert, Danny van Dyk

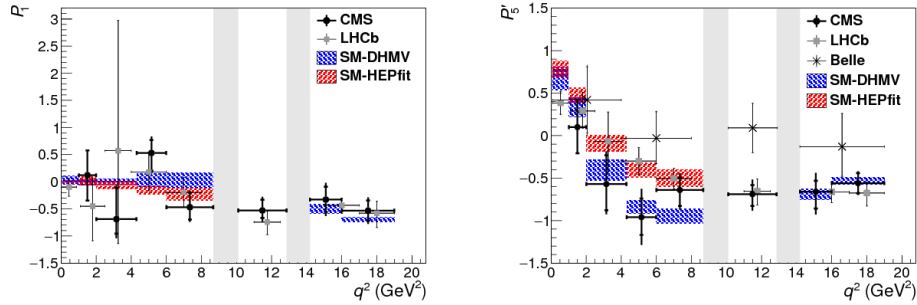


Fig. 6. Angular observables P_1 (left) and P'_5 (right) of $B^0 \rightarrow K^{*0} \mu^+ \mu^-$ decays depending on q^2 compared to the LHCb⁵⁰ and Belle⁵¹ measurements and with theory predictions overlaid (DHMV,^{45,52} HEPfit^{53,54}). The inner bars represent the statistical uncertainty, and the total uncertainty is illustrated by the outer vertical bars. The bin widths are indicated by the horizontal bars. Figures from.⁴⁸

charged muon in both B^0 and \bar{B}^0 decays, the angular distributions between theory and experiment differ. A translation scheme between the two conventions is given in.²⁴ More common than expressing the differential decay rates as functions of I_i and \bar{I}_i is using the CP -averaged and CP -asymmetric observables S_i and A_i as introduced in.³⁰

$$S_i = (I_i + \bar{I}_i) / \left(\frac{d\Gamma}{dq^2} + \frac{d\bar{\Gamma}}{dq^2} \right), \quad (18)$$

$$A_i = (I_i - \bar{I}_i) / \left(\frac{d\Gamma}{dq^2} + \frac{d\bar{\Gamma}}{dq^2} \right). \quad (19)$$

One can construct a complete set of observables $P_i^{(\prime)}$ with a reduced $B^0 \rightarrow K^*$ form-factor dependence⁴⁵⁻⁴⁷ in the large energy limit. They emerge from combinations of F_L and $S_3 - S_9$, where $P'_5 = S_5 / \sqrt{F_L(1 - F_L)}$ is the most notable and hence relevant for further discussions in this review.

In the angular analysis of $B^0 \rightarrow K^{*0} \mu^+ \mu^-$ decays by the CMS collaboration on a dataset of 20.5 fb^{-1} recorded in 2012, both P'_5 and $P_1 = 2S_3 / (1 - F_L)$ were determined,⁴⁸ by using a folded differential decay rate - an approach originally developed by the LHCb collaboration.^{37,49} After the folding, a multi-dimensional fit is performed, with the parameters of interest P_1 , P'_5 and A_5^5 along with signal and background yields, whereas the values of the longitudinal polarisation of the K^* meson, F_L , F_S and the interference between S- and P-wave, A_S , have been fixed to values determined in a previous analysis performed on the same dataset.³⁹ The results of P_1 and P'_5 are shown in Fig. 6 and are consistent with the SM predictions and previous measurements.

The aforementioned folding technique has also been employed by the Belle collaboration to extract P'_5 and $P'_4 = S_4 / \sqrt{F_L(1 - F_L)}$ from the full dataset for both $B^0 \rightarrow K^{*0} \mu^+ \mu^-$ and $B^0 \rightarrow K^{*0} e^+ e^-$ decays, as well as the combination of both

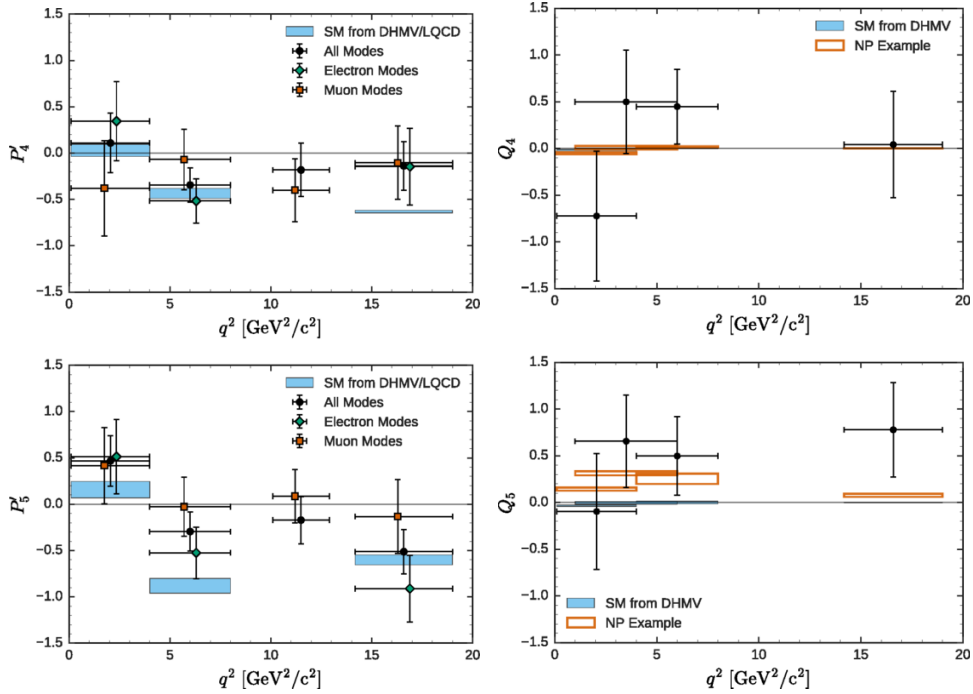


Fig. 7. Belle measurement of angular observables P'_4 (top left) and P'_5 (bottom left) depending on q^2 for $B^0 \rightarrow K^{*0} \ell^+ \ell^-$ with $\ell = e, \mu$ decays with theory predictions overlaid from DHMV⁵² and lattice QCD;⁵⁵ the measured values of Q_4 (top right) and Q_5 (bottom right) are compared to the DHMV prediction and an arbitrary new physics scenario (scenario 1 from ⁵²). Figures from.⁵¹

leptonic final states.⁵¹ The results on P'_4 and P'_5 are shown in Fig. 7. Tensions between measurement and SM prediction^{52,55} are observed for P'_5 for the muon final state in the region $4 \text{ GeV}^2/c^4 < q^2 < 8 \text{ GeV}^2/c^4$ of 2.6σ , whereas the electron mode differs by 1.3σ in the very same region, leading to a combined tension of 2.5σ . In addition to the $P'_{4,5}$ observables, the so-called $Q_{4,5} = P'_{4,5} - P'_{4,5}{}^e$ observables are determined for the first time; any deviation of these observables from zero would be a clear sign for new physics.⁵⁶ However in the Belle analysis, no deviation from zero is observed as can be seen in Fig. 7.

A more complete angular analysis was performed by the ATLAS collaboration on its 20.3 fb^{-1} dataset from 2012 by exploiting four different folding schemes allowing to extract a set of four observables for each scheme.⁵⁷ However neither S_9 nor A_{FB} can be measured with the chosen approach. The values for F_L and S_3 , which are common to each folding scheme, have been compared between the four fits and have found to be consistent. The publication comprises results on F_L , $S_{3,4,5,7,8}$, P_1 and $P'_{4,5,6,8}$, from which P'_4 and P'_5 are shown in Fig. 8. The obtained results are consistent with the different SM predictions within less than three standard deviations.

In contrast to previous analyses, the LHCb collaboration has performed a full

14 Johannes Albrecht, Stefanie Reichert, Danny van Dyk

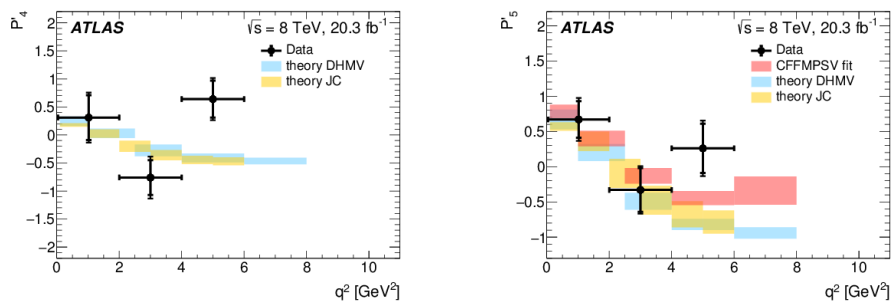


Fig. 8. Angular observables P'_4 (left) and P'_5 (right) depending on q^2 for $B^0 \rightarrow K^{*0} \mu^+ \mu^-$ decays with theory predictions overlaid from DHMV⁵² and JC.^{58,59} Figures from.⁵⁷

angular analysis, and has determined the set of angular observables by employing three different methods: by a maximum likelihood fit, by exploiting the angular principal moments,⁶⁰ and in addition the zero-crossing points of $S_{4,5}$ and A_{FB} were determined from a fit to the decay amplitudes.⁵⁰ The full angular analysis gives access to the correlation matrices, which provide crucial input for global fits to theoretical models. The results of the maximum likelihood and the method of angular principal moments are found to be compatible. As the maximum likelihood yields the most precise results, we restrict the discussion to this approach. However, we note in passing that the angular principal moments allow for smaller bin widths in q^2 and therefore provide more information of the q^2 shape of the angular observables compared to the maximum likelihood method. In this analysis performed by the LHCb collaboration, the fraction of the S-wave component was taken into account. Neglecting theoretical correlations, the S_i observables appear to be compatible with the SM predictions. The theory correlations can be displayed best in the space of the $P^{(\prime)}$ observables with the most notable deviation of the SM in P'_5 as can be seen from Fig. 9: in the regions $4 \text{ GeV}^2/c^4 < q^2 < 6 \text{ GeV}^2/c^4$ and $6 \text{ GeV}^2/c^4 < q^2 < 8 \text{ GeV}^2/c^4$, deviations of the measured values from the SM prediction⁶¹ of 2.8σ and 3.0σ can be observed, respectively. This confirms the tension seen in a previous LHCb analysis⁴⁹ in the region $4.30 \text{ GeV}^2/c^4 < q^2 < 8.68 \text{ GeV}^2/c^4$, which had a local significance of 3.7σ .

A fit to the complete set of CP -averaged observables, namely F_L , A_{FB} and $S_3 - S_9$, as determined from the maximum likelihood fit is performed by the LHCb collaboration⁵⁰ using the EOS software package^{62,63} for observables in the q^2 ranges below $8 \text{ GeV}^2/c^4$ and $15.0 \text{ GeV}^2/c^4 < q^2 < 19.0 \text{ GeV}^2/c^4$. The fit result illustrated in Fig. 10 indicates a tension of 3.4σ between the measurements and the SM prediction of $B^0 \rightarrow K^{*0} \mu^+ \mu^-$ alone.

When the fully differential decay rate (see Eq. (16)) is integrated over θ_ℓ and ϕ , the resulting expression depends on F_L and A_{FB} , which is what the BaBar collaboration exploited to measure those parameters⁶⁴ on their full dataset and to extract $P_2 = -2A_{FB}/(3[1 - F_L])$. The studied decay channels include not only

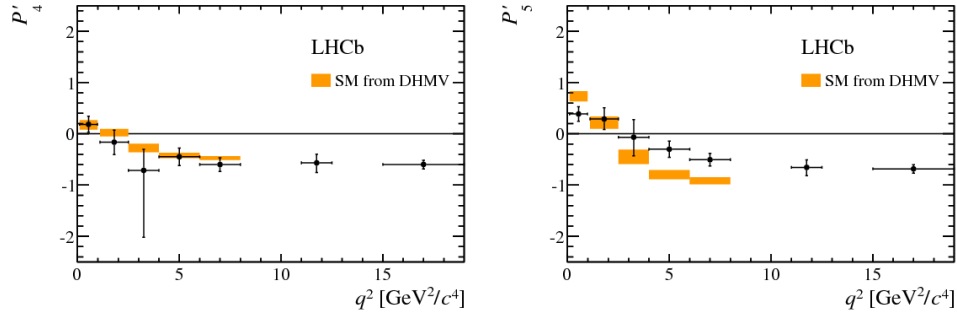


Fig. 9. Angular observables P'_4 (left) and P'_5 (right) of $B^0 \rightarrow K^{*0} \mu^+ \mu^-$ decays depending on q^2 as extracted from a maximum likelihood fit with theory predictions overlaid.⁶¹ Figures from.⁵⁰

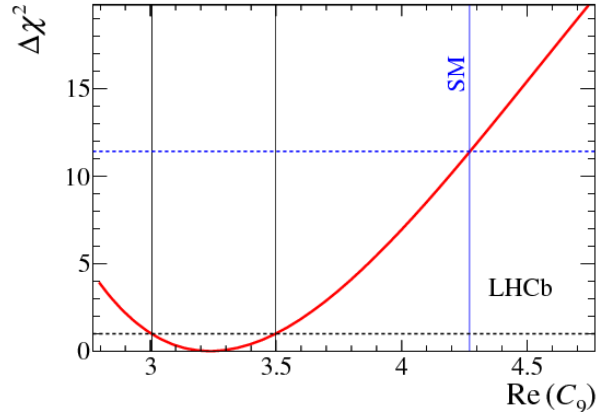


Fig. 10. The $\Delta\chi^2$ distribution for $\mathcal{R}e C_9^{\text{NP}\mu\mu}$ from a global fit to the full set of CP -averaged observables. The best fit point lies at $\mathcal{R}e\Delta C_9 = -1.04 \pm 0.25$, whereas the central value of the SM prediction is at $\mathcal{R}e C_9 = 4.27$,¹² hence indicating a tension of the measurement with respect to the SM prediction. Figures from⁵⁰ using the EOS software package.^{62,63}

$B^0 \rightarrow K^{*0} \mu^+ \mu^-$ and $B^0 \rightarrow K^{*0} e^+ e^-$ decays but also their charged counterparts. The results are summarised in Fig. 11 and most results are compatible amongst each other and with the SM prediction. In the low q^2 region, a tension is observed in F_L between $B^+ \rightarrow K^{*+} \ell^+ \ell^-$ and $B^0 \rightarrow K^{*0} \ell^+ \ell^-$ decays as well as the SM prediction. In the same region, there appears to be a small tension for P_2 .

Although most previous analyses focus on the muonic final states, several analyses measure *e.g.* the branching fraction or angular observables for $B^0 \rightarrow K^{*0} e^+ e^-$

^dThis result was later retracted in 2015.

16 Johannes Albrecht, Stefanie Reichert, Danny van Dyk

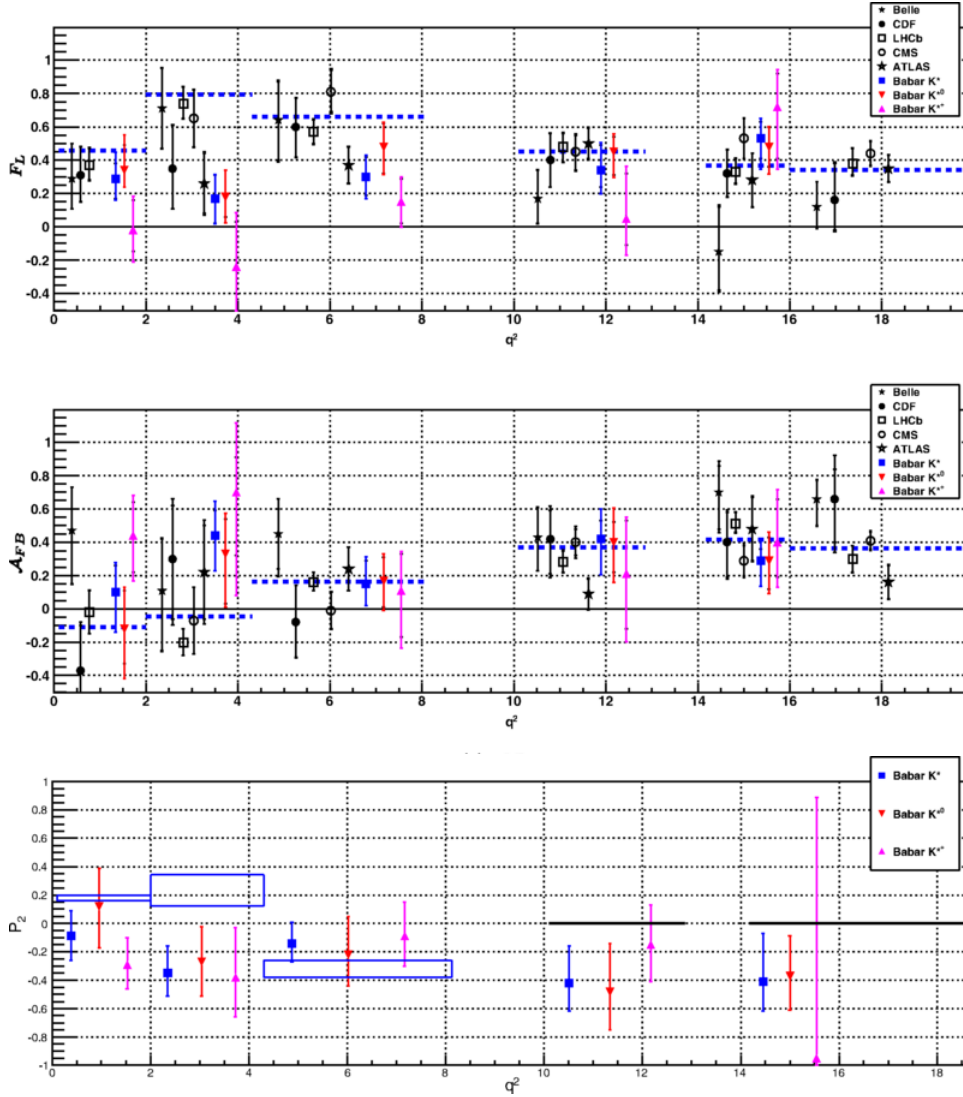


Fig. 11. Results for F_L (top), A_{FB} (middle) and P_2 (bottom) for different bins in q^2 . The results on F_L and A_{FB} are compared to previous results from Belle,⁶⁵ CDF,⁶⁶ LHCb,³⁷ CMS⁶⁷ and ATLAS⁶⁸ and the SM prediction⁶¹ (blue dashed line). For P_2 , the SM prediction⁶¹ is indicated by the blue boxes, which is only available in the low q^2 region, and hence in the high q^2 regions, the bin size is illustrated by the black lines. Figures from.⁶⁴

decays. On the 2011 LHCb dataset corresponding to 1fb^{-1} , the branching fraction of the electron mode has been determined in the dielectron mass range $30 - 1000\text{MeV}/c^2$ to be $\mathcal{B}(B^0 \rightarrow K^{*0}e^+e^-)_{30-1000\text{MeV}/c^2} = (3.1_{-0.8}^{+0.9} \pm 0.2) \cdot 10^{-7}$,⁶⁹ where the uncertainties are statistical, systematic and from the normalisation mode. This result is found to agree with SM predictions. On the 3fb^{-1} dataset, an an-

gular analysis has been performed⁷⁰ in the effective range $0.002 \text{ GeV}^2/c^4 < q^2 < 1.120 \text{ GeV}^2/c^4$ yielding

$$F_L = +0.16 \pm 0.06 \pm 0.03, \quad (20)$$

$$P_1 = A_T^{(2)} = -0.23 \pm 0.23 \pm 0.05, \quad (21)$$

$$A_T^{\mathcal{I}m} = +0.14 \pm 0.22 \pm 0.05, \quad (22)$$

$$A_T^{\mathcal{R}e} = +0.10 \pm 0.18 \pm 0.05, \quad (23)$$

where the uncertainties are statistical and systematic, respectively, and these results are in agreement with the SM expectations.

3.1.3. $B \rightarrow K^* \ell^+ \ell^-$ decays beyond the ground state

Apart from kaon and K^* states, one can consider higher K^* resonances above the $K^{*0}(892)$ mass range. The LHCb collaboration reported the first observation of the decay channels $B^+ \rightarrow K^+ \pi^+ \pi^- \mu^+ \mu^-$ and $B^+ \rightarrow \phi K^+ \mu^+ \mu^-$, whose branching fractions are

$$\mathcal{B}(B^+ \rightarrow K^+ \pi^+ \pi^- \mu^+ \mu^-) = (4.36_{-0.27}^{+0.29} \pm 0.21 \pm 0.18) \cdot 10^{-7}, \quad (24)$$

$$\mathcal{B}(B^+ \rightarrow \phi K^+ \mu^+ \mu^-) = (0.82_{-0.17}^{+0.19} {}_{-0.04}^{+0.10} \pm 0.27) \cdot 10^{-7}, \quad (25)$$

where the uncertainties are statistical, systematic and originating from the normalisation mode.⁷¹ For the $B^+ \rightarrow K^+ \pi^+ \pi^- \mu^+ \mu^-$ channel, the differential branching fractions illustrated in Fig. 12 could be measured.

In the region above the $K^{*0}(892)$ mass around $1430 \text{ MeV}/c^2$, the following resonances decaying to a $K^+ \pi^-$ final state contribute to the spectrum: the S-wave $K_0^*(1430)^0$, the P-waves $K^*(1410)^0$ and $K^*(1680)^0$ and the D-wave $K_2^*(1430)^0$. The LHCb collaboration has, for the first time, studied the differential branching fraction of the decay $B^0 \rightarrow K^+ \pi^- \mu^+ \mu^-$ and performed a full angular analysis including S-, P-, and D-wave contributions in the region $1330 \text{ MeV}/c^2 < m(K^+ \pi^-) < 1530 \text{ MeV}/c^2$.⁷² The former results are shown in Fig. 12; the latter results on the angular observables point towards large interference effects between the S-, P- and D-wave contributions. The fraction of the D-wave was estimated to be smaller than $F_D < 0.29$ at 95% C. L..⁷²

3.1.4. $B_s^0 \rightarrow \phi \ell^+ \ell^-$ decays

To gain further insight into the observed tensions in $b \rightarrow s \ell^+ \ell^-$ decays, B_s^0 decays were studied to complement studies of B^0 decays. In the decay channel $B_s^0 \rightarrow \phi \mu^+ \mu^-$, a full time-integrated angular analysis in line with the previously mentioned $B^0 \rightarrow K^{*0} \mu^+ \mu^-$ study has been performed. In contrast to the self-tagging $B^0 \rightarrow K^{*0} \mu^+ \mu^-$ decays, the ϕ meson decays into a pair of oppositely charged kaons, and hence is not flavour-specific, wherefore the accessible angular observables are F_L , the CP -averaged observables $S_{3,4,7}$ and the CP asymmetries $A_{5,6,8,9}$. For the

18 Johannes Albrecht, Stefanie Reichert, Danny van Dyk

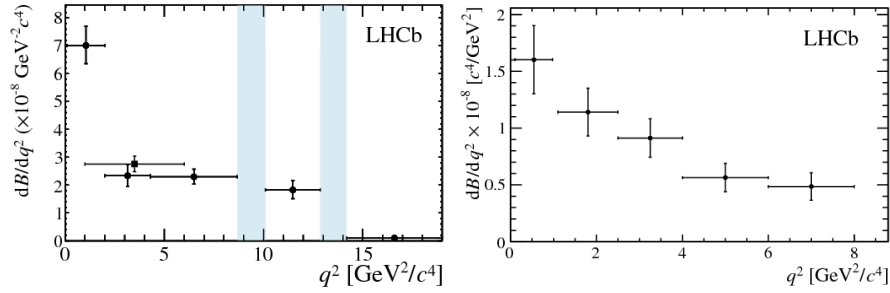


Fig. 12. Differential branching fraction results depending on q^2 for $B^+ \rightarrow K^+\pi^+\pi^-\mu^+\mu^-$ decays (left - figure from⁷¹) and for $B^0 \rightarrow K^+\pi^-\mu^+\mu^-$ decays in the region $1330 \text{ MeV}/c^2 < m(K^+\pi^-) < 1530 \text{ MeV}/c^2$ (right - figure from⁷²).

first time, the observables S_4 (shown in Fig. 13) and S_7 have been measured. This LHCb analysis comprises a measurement of the differential branching fraction shown in Fig. 13 for which a discrepancy of 3.3σ between the measured branching fraction and the SM prediction in the region $1.0 \text{ GeV}^2/c^4 < q^2 < 6.0 \text{ GeV}^2/c^4$ is observed.⁷³ This confirms a tension seen in the branching fraction measured by the previous analysis⁷⁴ of about 3.1σ when comparing to more recent SM predictions^{42,75} than was referred to in the publication.

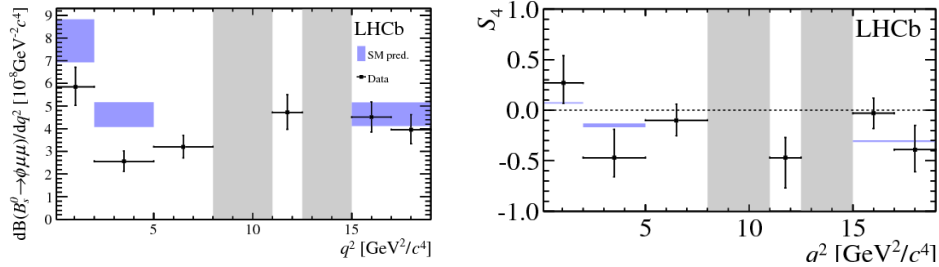


Fig. 13. Differential branching fraction results for $B_s^0 \rightarrow \phi\mu^+\mu^-$ decays depending on q^2 (left) and the angular observable S_4 (right) both with SM predictions overlaid.^{42,75} Figures from.⁷³

3.1.5. Sum of exclusive $b \rightarrow s\ell^+\ell^-$ decays

In contrast to the LHCb experiment, the B factories are able to perform inclusive measurements of *e.g.* $B \rightarrow X_s\ell^+\ell^-$ decays. However, inclusive analyses are challenging due to the required full reconstruction of the other B decay, which significantly reduces the efficiency. Hence, so-called sum-of-exclusive analyses are performed, which use a dominant subset of the corresponding exclusive decays instead. In an analysis of $B \rightarrow X_s\ell^+\ell^-$ decays with $\ell = e, \mu$ on the full BaBar dataset, ten dif-

ferent hadronic final states X_s were considered accounting in total for 70% of the fully inclusive rate.⁷⁶ In these overall twenty final states, the differential branching fraction of $B \rightarrow X_s \ell^+ \ell^-$ decays was measured and by extrapolating this sum-over-exclusive result, the inclusive branching fraction averaged over lepton flavours was determined to be

$$\mathcal{B}(B \rightarrow X_s \ell^+ \ell^-) = (6.73_{-0.64}^{+0.70} {}_{-0.25}^{+0.34} \pm 0.50) \cdot 10^{-6}, \quad (26)$$

for $q^2 > 0.1 \text{ GeV}^2/c^4$, where the uncertainties are statistical, systematic and originating from the model-dependent extrapolation. A slight excess of $\sim 2\sigma$ is observed in the high q^2 region of the partial branching fraction measurement shown in Fig. 14 for both electron and muon final states. From the branching fractions, which are determined for both electron and muon final states as well as the flavour-averaged combination, the direct CP asymmetry is extracted. By integrating over the q^2 region, the flavour-averaged CP asymmetry is found to be $\mathcal{A}_{CP}(B \rightarrow X_s \ell^+ \ell^-) = 0.04 \pm 0.11 \pm 0.01$, where the uncertainties are statistical and systematic, respectively,⁷⁶ and \mathcal{A}_{CP} is consistent with the SM prediction as are the CP asymmetries in bins of q^2 .

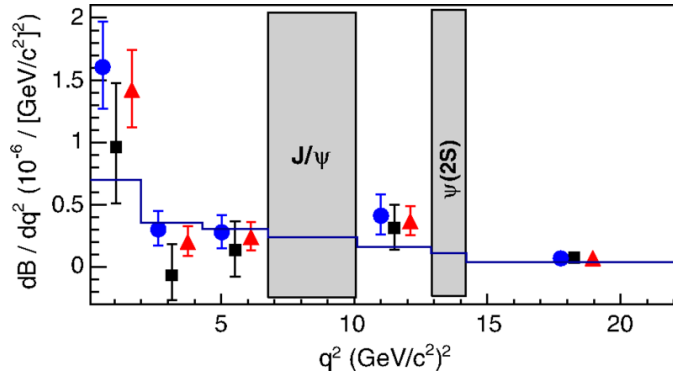


Fig. 14. Differential branching fraction results for $B \rightarrow X_s \ell^+ \ell^-$ decays for electron and muon final states as well as for the flavour-average depending on q^2 with SM predictions overlaid. Figure from.⁷⁶ Due to an inconvenient choice of scales, the $\sim 2\sigma$ excess at high q^2 is not visible.

A similar analysis was published by the Belle collaboration on its full dataset, in which the first measurement of A_{FB} as a function of q^2 was reported,⁷⁷ where the reconstruction of the hadronic system extends over ten final states. The sum-of-exclusive results are compatible with SM predictions as can be seen from Fig. 15. For $q^2 > 10.2 \text{ GeV}^2/c^4$, $A_{FB} < 0$ is excluded at a level of 2.3σ .

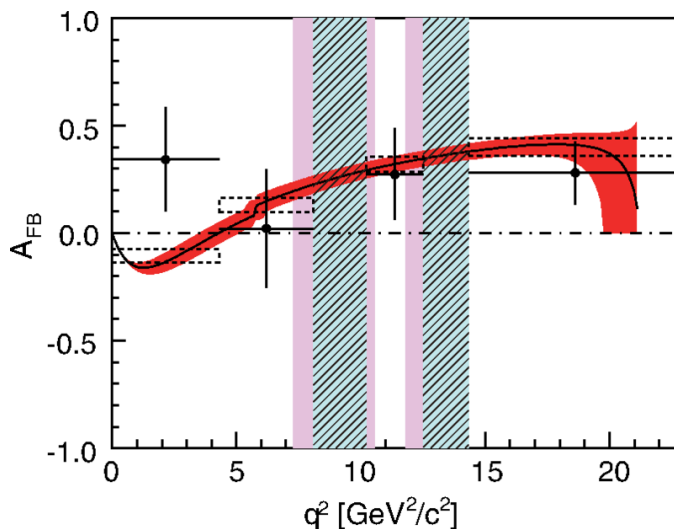


Fig. 15. Forward-backward asymmetry results for $B \rightarrow X_s \ell^+ \ell^-$ decays determined from a sum-of-exclusive approach depending on q^2 with SM predictions overlaid (red band with black curve and boxes). Figure from.⁷⁷

3.1.6. $\Lambda_b^0 \rightarrow \Lambda \ell^+ \ell^-$ decays

The $b \rightarrow s \ell^+ \ell^-$ transitions have also been studied in decays of Λ_b^0 baryons. Their decay to a ground state Λ baryons offers a rich phenomenology with ten angular observables in the case of an unpolarised Λ_b^0 baryon.⁷⁸ The LHCb collaboration has measured the differential branching fraction of $\Lambda_b^0 \rightarrow \Lambda \mu^+ \mu^-$ with $\Lambda \rightarrow p \pi^-$ decays along with the forward-backward asymmetries of the dimuon and the $p\pi$ systems denoted by A_{FB}^ℓ and A_{FB}^h , respectively, as well as the fraction of the longitudinally polarised dimuons, f_L .⁷⁹ The first significance of a signal is reported in the two regions $0.1 \text{ GeV}^2/c^4 < q^2 < 2.0 \text{ GeV}^2/c^4$ and between the charmonium resonances in the range $11.0 \text{ GeV}^2/c^4 < q^2 < 12.5 \text{ GeV}^2/c^4$. The angular observables f_L and A_{FB}^ℓ are extracted from a fit to the one-dimensional angular distributions as a function of $\cos \theta_\ell$, which is defined as the angle between the positive (negative) muon and dimuon flight direction in the Λ_b^0 ($\bar{\Lambda}_b^0$) rest frame. Similarly, the hadronic forward-backward asymmetry is determined from the one-dimensional distribution of $\cos \theta_h$, where θ_h is the angle between the proton and Λ directions. The results on A_{FB}^h are in good agreement with the SM prediction, whereas the leptonic forward-backward asymmetry lies systematically above the prediction. The results on A_{FB} along with the differential branching fraction are depicted in Fig. 16. The interpretation of these data is challenging and no convincing simultaneous theory explanation of these data and the anomalies in the mesonic modes has been found.⁸⁰

For a subset of the angular observables the impact of all dimension-six NP contributions has been worked out in.⁸² With the future dataset of the LHCb detector, a novel test of the SM could be carried out by studies of polarised versus unpolarised

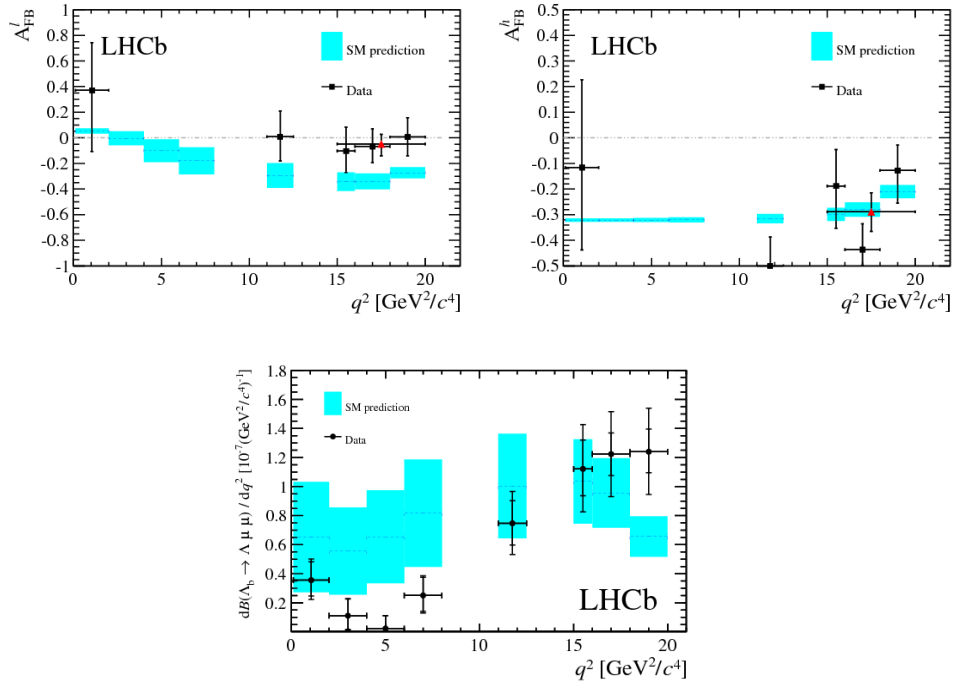


Fig. 16. Results for A_{FB} of the leptonic system (top left) and hadronic system (top right) and the differential branching fraction (bottom) in $\Lambda_b^0 \rightarrow p \mu^- \nu$ decays. The SM predictions⁸¹ are overlaid as band. Figures from.⁷⁹

$\Lambda_b^0 \rightarrow \Lambda \ell^+ \ell^-$ decays,⁸³ where the number of angular observables increases from 10 in the unpolarised case to 34 in the case of a non-zero production polarisation of the Λ_b^0 baryons.

3.1.7. Tests of lepton flavour universality

A very clean test for new physics in $b \rightarrow s \ell^+ \ell^-$ decays can be performed by taking ratios of branching fractions to different lepton species in the final state or by measuring the difference of angular observables across lepton species, *e.g.* in Q_5 as has been discussed in Section 3.1.2. Here, the prediction of lepton flavour universality (LFU) is probed, *i.e.* the SM prediction that weak couplings to all lepton flavours are identical. At the current experiments, $b \rightarrow s \ell^+ \ell^-$ decays with electrons and muons in the final state are accessible. For q^2 larger than 1 GeV^2 both muons and electrons are sufficiently relativistic such that uncertainties in the hadronic form factors cancel to a very good approximation leaving a SM prediction with uncertainties well below 1%.⁸⁴ Log-enhanced radiative corrections for the decay rates are discussed in⁸⁵ yielding a larger uncertainty $\sim 1\%$.

In recent years, the interest in lepton flavour universality tests has increased,

mainly driven by two measurements of the LHCb collaboration: the ratio of $B^+ \rightarrow K^+ \mu^+ \mu^-$ to $B^+ \rightarrow K^+ e^+ e^-$, called $R(K)$,⁸⁶ and the ratio of $B^0 \rightarrow K^{*0} \mu^+ \mu^-$ to $B^0 \rightarrow K^{*0} e^+ e^-$, called $R(K^*)$.⁸⁷ The LHCb collaboration uses basically the same strategy for both analyses, that is discussed here for general $b \rightarrow s \ell^+ \ell^-$ decays with the corresponding hadron H . The lepton flavour universality testing ratio $R(H)$ is then defined as⁸⁴

$$R(H) = \frac{\int \frac{d\Gamma(B \rightarrow H \mu^+ \mu^-)}{dq^2} dq^2}{\int \frac{d\Gamma(B \rightarrow H e^+ e^-)}{dq^2} dq^2}, \quad (27)$$

where the differential decay rate is measured in certain q^2 ranges driven by experimental constraints and theoretical interests. The q^2 range corresponding to the J/ψ and $\psi(2S)$ is always excluded from the LFU analysis but used as control and normalisation channel, since they are tested to be lepton-flavour universal to very high precision.⁸⁸ To cancel experimental uncertainties in the absolute efficiencies of the measurements, the ratio $R(H)$ is not measured directly but as double ratio normalising the non-resonant signal mode to the corresponding high-statistics resonant mode, let us consider a J/ψ resonance in the following. The ratio $R(H)$ is then measured as

$$R(H) = \frac{\mathcal{B}(B \rightarrow H \mu^+ \mu^-)}{\mathcal{B}(B \rightarrow H J/\psi (\rightarrow \mu^+ \mu^-))} \bigg/ \frac{\mathcal{B}(B \rightarrow H e^+ e^-)}{\mathcal{B}(B \rightarrow H J/\psi (\rightarrow e^+ e^-))}. \quad (28)$$

A few comments are in order to explain this experimental strategy: first, this method tests for LFU violations in FCNC decays and it relies on the conservation of LFU in the corresponding resonant decay modes. To test this assumption, the ratio of the branching fractions in the resonant channel

$$r(J/\psi) = \frac{\mathcal{B}(B \rightarrow H J/\psi (\rightarrow \mu^+ \mu^-))}{\mathcal{B}(B \rightarrow H J/\psi (\rightarrow e^+ e^-))}, \quad (29)$$

is confirmed to agree with the conservation of lepton flavour universality. It has to be stressed that this test is more stringent than required because it cross-checks the absolute ratio of muon to electron reconstruction, identification and selection efficiencies while in the double-ratio of $R(H)$ only relative efficiencies between non-resonant and resonant channel matter. The entire range of q^2 can be tested with this method, if the ratio $r(J/\psi)$ is measured in bins of the daughter particle momenta.

The most precise measurement of $r(J/\psi)$ has been performed in LHCb's analysis of $R(K^*)$, where it was found to be in agreement with unity with a precision of 4.5%. Compared to the statistical uncertainties of the LFU tests of the order of 10%, this uncertainty is subdominant. For further tests with enlarged datasets, the precision in the determination of efficiencies as cross-checked in $r(J/\psi)$ needs to be studied in greater detail.

Among the $b \rightarrow s \ell^+ \ell^-$ decays, the $B^+ \rightarrow K^+ \ell^+ \ell^-$ mode is best accessible to the LHCb experiment and the B factories. The former collaboration has published

a measurement using the full Run 1 dataset.⁸⁶ The value of $R(K)$ is found to be

$$R(K) = 0.745_{-0.074}^{+0.090} \pm 0.036, \quad (30)$$

where the uncertainties are statistical and systematic, and this measurement constitutes a tension with the SM prediction³² of 2.6 standard deviations. The BaBar and Belle experiments have also performed tests of lepton flavour universality^{65,89} but their analysed dataset is much smaller than the LHCb dataset and hence the measurement has significantly increased uncertainties. The status of all measurements is summarised in Fig. 17.

Further tests of LFU have been carried out with a K^{*0} resonance in the final state; a study in $B^0 \rightarrow K^{*0} \ell^+ \ell^-$ decays was published recently by the LHCb collaboration in two bins of q^2 . The results in both q^2 ranges are found below the SM prediction at

$$R(K^*) = \begin{cases} 0.66_{-0.07}^{+0.11} \pm 0.03 & \text{for } 0.045 \text{ GeV}^2/c^4 < q^2 < 1.1 \text{ GeV}^2/c^4, \\ 0.69_{-0.07}^{+0.11} \pm 0.05 & \text{for } 1.1 \text{ GeV}^2/c^4 < q^2 < 6.0 \text{ GeV}^2/c^4, \end{cases} \quad (31)$$

where the uncertainties are statistical and systematic, respectively. The measurement of $R(K^*)$ is shown in Fig. 17. The significances of the deviation of the SM expectation is 2.1-2.3 and 2.4-2.5 standard deviations, respectively. The SM prediction for $R(K^*)$ in the lowest bin suffers from an additional source of theoretical uncertainty due to LFU-violating SM effects. These effects can for example stem from almost on-shell hadronic intermediate states that decay at different rates into muons versus electrons. We refer to⁸⁵ for a discussion.

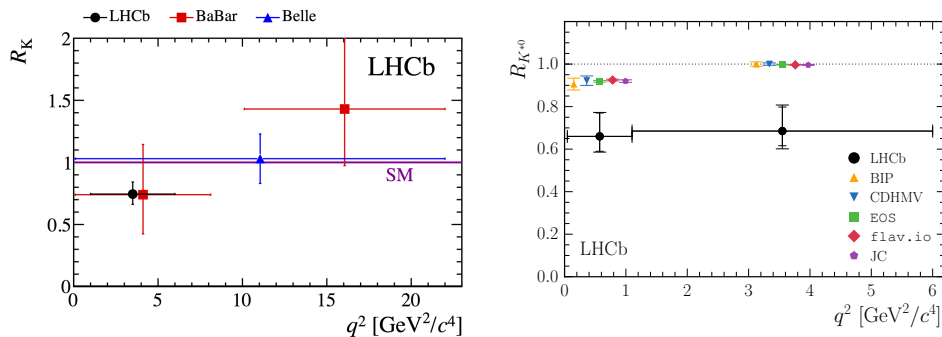


Fig. 17. Tests of LFU in $b \rightarrow s \ell^+ \ell^-$ decays: summary of the measurements of $R(K)$ of the LHCb, BaBar and Belle experiments with the SM prediction overlaid as a line at unity (left) and the LHCb measurement of $R(K^*)$ together with several SM predictions (right) are shown. Figures from.^{86,87}

The data that the LHCb experiment has collected at the point of this review contains already a factor three more beauty mesons than in the published LFU analyses on 3 fb^{-1} . With the increased sensitivity of the LHCb detector and the start

of the Belle II experiment, the tensions seen in the $R(K)$ and $R(K^*)$ measurements will be either confirmed or ruled out in the foreseeable future.

Additionally to the channels discussed above, LFU can be tested in $B_s^0 \rightarrow \phi \ell^+ \ell^-$ decays, where a first observation of the channel $B_s^0 \rightarrow \phi \ell^+ \ell^-$ should be possible already with 3 fb^{-1} of data at LHCb. Also $B^+ \rightarrow K^+ \pi^+ \pi^- \ell^+ \ell^-$ and $\Lambda_b^0 \rightarrow \Lambda^{(*)} \ell^+ \ell^-$ decays are analysed to test for a potential violation of lepton universality. Combining the already collected large datasets and the analysis of more channels, the question if LFU is conserved in the SM should be conclusively answered in the near future. A quantitative analysis of the future sensitivities to discover LFU is discussed in Section 6.

3.2. A note on $b \rightarrow d \ell^+ \ell^-$ decays

In contrast to the well tested $b \rightarrow s \ell^+ \ell^-$ decays, that are described above in Section 3.1, the decays of the type $b \rightarrow d \ell^+ \ell^-$ are CKM suppressed by a factor of about 32.⁸⁸ The $b \rightarrow d \ell^+ \ell^-$ system is in principle unconnected to other systems, wherefore it provides a complementary probe for new physics effects *e.g.* for the *hypothesis of Minimal Flavour Violation*,⁹⁰ in which these two systems would be connected. Therefore, ratios of related decays provide a stringent test of this hypothesis.

The first $b \rightarrow d \ell^+ \ell^-$ decay that was observed⁹¹ is $B^+ \rightarrow \pi^+ \mu^+ \mu^-$, where the differential branching ratio was measured with about one hundred candidates, see Fig. 18, and the total branching fraction is found to be $\mathcal{B}(B^+ \rightarrow \pi^+ \mu^+ \mu^-) = (1.83 \pm 0.24 \pm 0.05) \cdot 10^{-8}$, where the uncertainties are of statistical and systematic nature. The publication includes the first test of CP violation in this decay with the CP asymmetry being $\mathcal{A}_{CP}(B^+ \rightarrow \pi^+ \mu^+ \mu^-) = -0.11 \pm 0.12 \pm 0.01$ where the uncertainties refer to statistical and systematic uncertainties. Both the differential decay rate and the CP asymmetry are consistent with SM expectations.

The decays $B_{s,d} \rightarrow \pi^+ \pi^- \mu^+ \mu^-$ have also been measured by the LHCb collaboration.⁹² However, the interpretation of these decays is more difficult as the hadronically complex structure of the $\pi^+ \pi^-$ system needs to be considered. The reconstructed $\pi^+ \pi^- \mu^+ \mu^-$ mass distribution shown in Fig. 18, illustrates this point clearly. In the dipion range of $0.5 - 1.3 \text{ GeV}/c^2$, the first observation of the decay $B_s^0 \rightarrow \pi^+ \pi^- \mu^+ \mu^-$ with a branching fraction of $\mathcal{B}(B_s^0 \rightarrow \pi^+ \pi^- \mu^+ \mu^-) = (8.6 \pm 1.5 \pm 0.7 \pm 0.7) \cdot 10^{-8}$ and the first evidence for the decay $B^0 \rightarrow \pi^+ \pi^- \mu^+ \mu^-$ with a branching fraction of $\mathcal{B}(B^0 \rightarrow \pi^+ \pi^- \mu^+ \mu^-) = (2.11 \pm 0.51 \pm 0.15 \pm 0.16) \cdot 10^{-8}$ with the uncertainties being statistical, systematic and originating from the normalisation channel were reported.⁹²

An evidence for the decay $B_s^0 \rightarrow \bar{K}^{*0} \mu^+ \mu^-$ has recently been seen by the LHCb collaboration,⁹³ using a total dataset of 4.6 fb^{-1} of collision data at $\sqrt{s}=7, 8,$ and 13 TeV . The significance of this evidence is found to be 3.4 standard deviations.

In the future, the importance of studies of the decay $b \rightarrow d \ell^+ \ell^-$ will significantly increase as it allows to measure the same effects as observed in $b \rightarrow s \ell^+ \ell^-$ decays

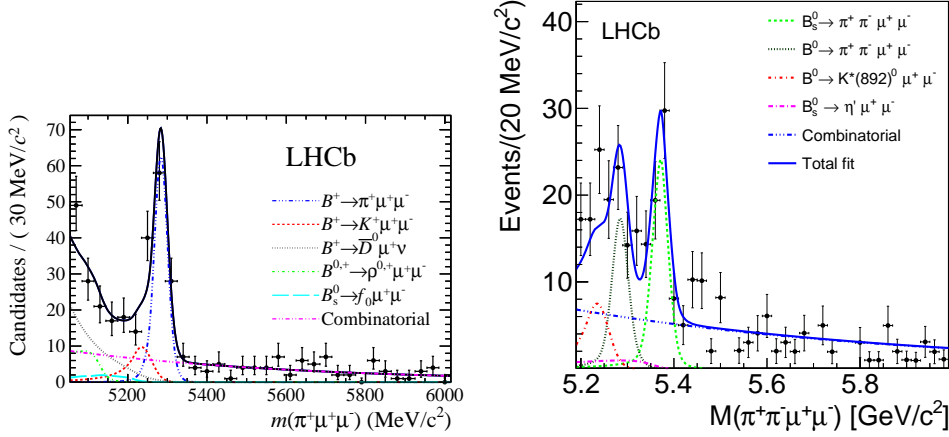


Fig. 18. Fit to the invariant mass distribution of $B^+ \rightarrow \pi^+ \mu^+ \mu^-$ (left); the separate fit to the charge-conjugated sample is omitted here for reasons of brevity. Fit to the invariant mass distribution of $B_{s,d} \rightarrow \pi^+ \pi^- \mu^+ \mu^-$ candidates (right), where the small contributions from $B_s^0 \rightarrow \phi \mu^+ \mu^-$ and $B^+ \rightarrow K^+ \mu^+ \mu^-$ are not visible. Figures taken from⁹¹ and⁹² respectively.

and thus constitute an independent verification channel. Furthermore, ratios of $b \rightarrow d \ell^+ \ell^-$ and $b \rightarrow s \ell^+ \ell^-$ decays provide stringent tests of the flavour structure of the underlying interactions and allow to study the hypothesis of minimal flavour violation.⁹⁰

3.3. Leptonic rare $B_{(s)}^0 \rightarrow \ell^+ \ell^-$ decays

In 1985, the CLEO collaboration published the first limit on $B^0 \rightarrow \mu^+ \mu^-$, whereas UA1 should follow four years later with the first limit in the $B_s^0 \rightarrow \mu^+ \mu^-$ channel; the timeline of limits and measurements is shown in Fig. 19. In recent years, the interest in the decays $B_{(s)}^0 \rightarrow \mu^+ \mu^-$ increased as the SM rate came into experimental reach. The SM prediction for the decay $B_s^0 \rightarrow \mu^+ \mu^-$ is known with a precision better than 5% as discussed in detail in Section 4.3 and lies at $\mathcal{B}_{\text{SM}}(B_s^0 \rightarrow \mu^+ \mu^-) = (3.57 \pm 0.17) \cdot 10^{-9}$.⁹⁴ It has to be noted that the experimentally accessible observable is the time integrated branching fraction, which differs from the theoretical branching fraction at $t = 0$ ⁹⁵ due to B_s^0 mixing effects. The $B_s^0 \rightarrow \ell^+ \ell^-$ branching fractions discussed in this chapter are all the time integrated quantities. Due to the very small width difference, this effect is negligible for B^0 decays.

The corresponding decay $B^0 \rightarrow \mu^+ \mu^-$ is additionally CKM-suppressed and therefore has an SM rate a factor 32 lower than the B_s^0 decay. Analysing the sensitivity in NP physics, these modes are particularly interesting to look for new scalar or pseudo-scalar interactions, *e.g.* in two Higgs doublet models (2HDM) type II^{96,97} large effects are predicted.

In 2012, the LHCb collaboration reported a first evidence of the branching ratio of $B_s^0 \rightarrow \mu^+ \mu^-$, measured to $\mathcal{B}(B_s^0 \rightarrow \mu^+ \mu^-) = (2.9_{-1.0}^{+1.1}) \cdot 10^{-9}$ with a

significance of 4.0 standard deviations.⁹⁸ The first observation of this decay, exceeding six standard deviations, has been achieved by a joint analysis of the CMS and LHCb collaborations,⁹⁹ where the branching ratio was determined to be $\mathcal{B}(B_s^0 \rightarrow \mu^+ \mu^-) = (2.8_{-0.6}^{+0.7}) \cdot 10^{-9}$. The ATLAS collaboration also published an analysis of 2011 and 2012 data¹⁰⁰ with a smaller sensitivity than the CMS or LHCb collaborations. No significant signal was neither expected nor seen. The compatibility of the measurement with the SM prediction was found to be at the level of 2.0σ . The first single experiment observation of $B_s^0 \rightarrow \mu^+ \mu^-$ was reported in 2017 by the LHCb collaboration of $\mathcal{B}(B_s^0 \rightarrow \mu^+ \mu^-) = (3.0 \pm 0.6_{-0.2}^{+0.3}) \cdot 10^{-9}$ with a significance of 7.8 standard deviations partly exploiting data from the LHC's Run 2.¹⁰¹ In addition to the branching ratio, the first measurement of the effective lifetime of the B_s^0 meson, $\tau(B_s^0 \rightarrow \mu^+ \mu^-) = (2.04 \pm 0.44 \pm 0.05)$ ps was published, which is related to the parameter

$$A_{\Delta\Gamma}^{\mu^+\mu^-} = -\frac{2\Re(\lambda)}{1 + |\lambda|^2} \quad \text{with} \quad \lambda = \frac{q \mathcal{A}(\bar{B}_s^0 \rightarrow \mu^+ \mu^-)}{p \mathcal{A}(B_s^0 \rightarrow \mu^+ \mu^-)}, \quad (32)$$

with the complex coefficients p and q connecting mass and flavour eigenstates in the $B_s^0 - \bar{B}_s^0$ system, and \mathcal{A} referring to the decay amplitudes of the respective process. In certain NP models, $A_{\Delta\Gamma}^{\mu^+\mu^-}$ ranges between $[-1, 1]$. In the SM, only a pseudo-scalar amplitude is allowed and hence $A_{\Delta\Gamma}^{\mu^+\mu^-} \approx 1 - 1.0 \cdot 10^{-5}$; the deviation of unity is caused by power-enhanced QED corrections.⁹⁴ The effective lifetime $\tau(B_s^0 \rightarrow \mu^+ \mu^-)$ is an orthogonal probe of NP models compared to the $B_s^0 \rightarrow \mu^+ \mu^-$ branching fraction as it is sensitive to models predicting the branching fraction close to its SM value. However, the current experimental sensitivity is insufficient to make a definitive statement on the validity of the SM or NP models, but $\tau(B_s^0 \rightarrow \mu^+ \mu^-)$ will become more important in the future when larger datasets become available. The LHCb measurement is consistent with the hypothesis of $A_{\Delta\Gamma}^{\mu^+\mu^-} = +1(-1)$ at 1.0 (1.4) standard deviations.

The experimental results discussed in Section 3.1.7 hint at a violation of Lepton Flavour Universality, therefore the non-muonic decays $B_s^0 \rightarrow e^+ e^-$ and $B_s^0 \rightarrow \tau^+ \tau^-$ offer an orthogonal probe for NP. Some models predict an enhancement of $B_s^0 \rightarrow e^+ e^-$ over $B_s^0 \rightarrow \mu^+ \mu^-$ proportional to m_μ/m_e .¹⁰³ Also the branching fraction of the decay $B_s^0 \rightarrow \tau^+ \tau^-$ could be enhanced with respect to the SM prediction by several orders of magnitude.^{104, 105}

Experimentally, both $B_{(s)} \rightarrow e^+ e^-$ and $B_{(s)} \rightarrow \tau^+ \tau^-$ final states are more challenging than the muonic mode: when reconstructing the di-electron final state, bremsstrahlung photons have to be accounted for, and hence the mass resolution is significantly degraded and the physical backgrounds are more difficult to determine. In the tauonic decay channel, the decays of the τ leptons render the measurement challenging as they involve at least two neutrinos, and hence can only be reconstructed if additional information on the B momentum is available.

The current world's best upper limits on $B_{(s)} \rightarrow e^+ e^-$ stem from the CDF

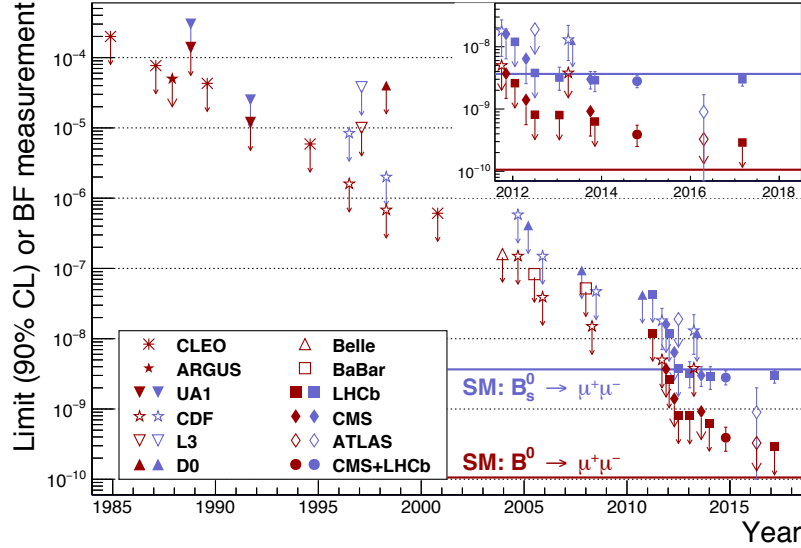


Fig. 19. Development of limits and branching fraction measurements of the decays $B_s^0 \rightarrow \mu^+\mu^-$ (blue) and $B^0 \rightarrow \mu^+\mu^-$ (red) over time. Figure from,⁹⁹ updated in.¹⁰²

collaboration,¹⁰⁶ which determined the following limits at 90% C.L.

$$\mathcal{B}(B_s^0 \rightarrow e^+e^-) < 2.8 \cdot 10^{-7}, \quad (33)$$

$$\mathcal{B}(B^0 \rightarrow e^+e^-) < 8.3 \cdot 10^{-8}. \quad (34)$$

The SM predictions are at the level of 10^{-13} (see¹⁰⁷) and hence not within experimental reach. Searches for $B_{(s)} \rightarrow e^+e^-$ are therefore a clean test for effects beyond the Standard Model, as no SM contribution is measurable and any observed signal would be a clean signal for New Physics. A search for $B_s^0 \rightarrow e^+e^-$ using the LHCb data is in preparation.

A first upper limit on $B_s^0 \rightarrow \tau^+\tau^-$ was recently published by the LHCb collaboration¹⁰⁸ together with a limit on $B^0 \rightarrow \tau^+\tau^-$ improving the previous limits. The limits at 95% C.L. are

$$\mathcal{B}(B_s^0 \rightarrow \tau^+\tau^-) < 6.8 \cdot 10^{-3}, \quad (35)$$

$$\mathcal{B}(B^0 \rightarrow \tau^+\tau^-) < 2.1 \cdot 10^{-3}, \quad (36)$$

whereas the SM predictions are around four to five orders of magnitude below the current experimental sensitivity at $\mathcal{B}(B_s^0 \rightarrow \tau^+\tau^-) = (7.73 \pm 0.49) \cdot 10^{-7}$ and $\mathcal{B}(B^0 \rightarrow \tau^+\tau^-) = (2.22 \pm 0.19) \cdot 10^{-8}$, respectively.¹⁰⁷ Therefore, also in $B_{(s)} \rightarrow \tau^+\tau^-$ decays, any observed signal would be a clear sign of New Physics. The sensitivity of $B_{(s)} \rightarrow \tau^+\tau^-$ decays is expected to greatly improve in the upgrade of the LHCb experiment, profiting from the improvements in the trigger strategy.

3.4. Exclusive $b \rightarrow s\gamma$ decays

Over the past years, the advancements in exclusive $b \rightarrow s\gamma$ decays have been sparse, and other reviews, see *e.g.*,¹⁰⁹ summarise the measurements by the B factories, wherefore we restrict this review to the most recent measurements. The Belle collaboration reported a measurement of the $B \rightarrow K^*\gamma$ branching fractions, $\mathcal{B}(B^0 \rightarrow K^{*0}\gamma) = (3.96 \pm 0.07 \pm 0.14) \cdot 10^{-5}$ and $\mathcal{B}(B^+ \rightarrow K^{*+}\gamma) = (3.76 \pm 0.10 \pm 0.12) \cdot 10^{-5}$,¹¹⁰ which only place weak constraints on possible NP scenarios due to the large form factor uncertainties. Stronger constraints are obtained by measuring the direct CP asymmetry $\Delta\mathcal{A}^{CP} \equiv (\mathcal{A}^{CP}(B^+ \rightarrow K^{*+}\gamma) - \mathcal{A}^{CP}(B^0 \rightarrow K^{*0}\gamma)) = (2.4 \pm 2.8 \pm 0.5)\%$ with $\mathcal{A}^{CP}(B^0 \rightarrow K^{*0}\gamma) = (-1.3 \pm 1.7 \pm 0.4)\%$ and $\mathcal{A}^{CP}(B^+ \rightarrow K^{*+}\gamma) = (+1.1 \pm 2.3 \pm 0.3)\%$. The average of the CP asymmetries is $\mathcal{A}^{CP} = (-0.1 \pm 1.4 \pm 0.3)\%$.¹¹⁰ This result comprises, for the first time, evidence of isospin violation (defined similarly to Eq. (10)) at a significance of 3.1σ , $\Delta_{0+} = (+6.2 \pm 1.5 \pm 0.6 \pm 1.2)\%$, where the uncertainties are statistical, systematic and the third uncertainty arises from the production ratio of charged to neutral $b\bar{b}$ pairs;¹¹⁰ this result is consistent with the SM expectation. We recall that measurements of isospin asymmetries in the decays crucially depend on accurate determinations of isospin asymmetries in the production. The consequences of a bias-free determination of the production asymmetry and its consequences on Δ_{0+} are discussed in.¹¹¹ From the measured $B^0 \rightarrow K^{*0}\gamma$ branching fraction, comprising solely the charged $K^{*0} \rightarrow K^+\pi^-$ channel in order to reduce systematic uncertainties, the ratio

$$\frac{\mathcal{B}(B^0 \rightarrow K^{*0}\gamma)}{\mathcal{B}(B_s^0 \rightarrow \phi\gamma)} = 1.10 \pm 0.16 \pm 0.09 \pm 0.18, \quad (37)$$

was determined, where the uncertainties are statistical, systematic and the third uncertainty comes from the $B_s^{(*)0}\bar{B}_s^{(*)0}$ production in $\Upsilon(5S)$ decays.¹¹⁰ Here, the f_s related uncertainty arises from the measurement of $\mathcal{B}(B_s^0 \rightarrow \phi\gamma) = (3.6 \pm 0.5 \pm 0.3 \pm 0.6) \cdot 10^{-5}$.¹¹² The results on the $b \rightarrow s\gamma$ branching fraction ratio are consistent with both the SM expectations and the LHCb result.¹¹³ In $B_s^0 \rightarrow \phi\gamma$ decays, the photons are predominantly left-handed with a right-handed component suppressed by the ratio of the s to b masses, where the latter component could be enhanced NP scenarios. Information on the polarisation can for example be obtained from *e.g.* $B^0 \rightarrow K^{*0}e^+e^-$ decays (see Section 3.1 for details), which probe the photon polarisation at low q^2 , or from a measurement of the parameter A^Δ . The latter is a function of the left- and right-handed polarisation amplitudes given by $A^\Delta = \sin(2\Psi)$ with $\tan(\Psi) \equiv |A(\bar{B}_s^0 \rightarrow \phi\gamma_R)|/|A(\bar{B}_s^0 \rightarrow \phi\gamma_L)|$ in the SM. The LHCb collaboration has recently reported the first time-dependent measurement of a radiative B_s^0 decay, and has determined $A^\Delta = -0.98_{-0.52}^{+0.46} {}_{-0.20}^{+0.23}$ in $B_s^0 \rightarrow \phi\gamma$,¹¹⁴ which is consistent with the SM expectation within two standard deviations.

In contrast to $B_s^0 \rightarrow \phi\gamma$, the decay $B^0 \rightarrow \phi\gamma$ is heavily suppressed and the current most precise limit is reported by the Belle collaboration as $\mathcal{B}(B^0 \rightarrow \phi\gamma) <$

$1.0 \cdot 10^{-7}$ at 90% C.L.¹¹⁵ As this decay is not sensitive to the electromagnetic dipole operator O_7 but to the QCD-penguin operators O_{3-6} , we refrain from a more detailed discussion.

4. Theory of rare $b \rightarrow sl^+\ell^-$ decays

As discussed in Section 2, the description of rare b decays involves hadronic matrix elements of various local and non-local operators. We discuss these matrix elements in the following in Section 4.1 and Section 4.2. Subsequently in Section 4.3, we will revisit the theoretical foundations of the observables discussed in Section 3.

4.1. Hadronic matrix elements of local operators

For the purely leptonic decays of B_s mesons and at leading order in α_e , the only occurring hadronic matrix element emerges from the axialvector current

$$\langle 0 | \bar{s} \gamma^\mu \gamma_5 b | \bar{B}_s(p) \rangle \equiv ip^\mu f_{B_s}, \quad (38)$$

which introduces the B_s meson decay constant f_{B_s} . The hadronic matrix elements of the operators $O_{9,9',7,7'}$ are suppressed by one power of α_e ; see⁹⁴ for a recent study to that effect.

Presently, the only ab-initio method to obtain the B_s decay constant is lattice QCD. For a discussion of the inherent systematic uncertainties in lattice determinations of the decay constant we refer to the most recent version of the FLAG report.¹¹⁶ For determinations with $N_f = 2 + 1 + 1$ dynamical light quark flavours, there are presently three results by the European Twisted Mass collaboration (ETM),¹¹⁷ the HPQCD collaboration,¹¹⁸ and the Fermilab/MILC collaborations (FNAL/MILC).¹¹⁹ The lattice results read:

$$\begin{aligned} f_{B_s} &= 235 \pm 9 \text{ MeV} && \text{(ETM}^{117}\text{)}, \\ f_{B_s} &= 224 \pm 5 \text{ MeV} && \text{(HPQCD}^{118}\text{)}, \\ f_{B_s} &= 230.7 \pm 1.2 \text{ MeV} && \text{(FNAL/MILC}^{119}\text{)}. \end{aligned} \quad (39)$$

Besides lattice simulations, the decay constants are also accessible through QCD Sum Rules (QCDSR). The latter are based on an approach based on an Operator Product Expansion (OPE) of an inclusive quantity, and relating it to exclusive matrix elements in a dispersive framework. A large, and difficult-to-quantify systematic uncertainty arises from the use of quark-hadron duality. The QCDSR results are compatible with the lattice determination, albeit with uncertainties roughly one order of magnitude larger than the most precise lattice determination:

$$f_{B_s} = 234^{+15}_{-11} \text{ MeV} \quad \text{(QCDSR}^{120}\text{)}. \quad (40)$$

For the description of the semileptonic b -hadron decays, the matrix elements of the local operators are decomposed in terms of *form factors*: scalar-valued functions

of q^2 , the square of the momentum transfer to the dilepton system. A commonly used basis consists of three form factors f_+ , f_- , and f_T for transitions to a single pseudo-scalar meson (see *e.g.*¹²¹), or seven form factors V , $A_{0,1,2}$, $T_{1,2,3}$ for transitions to a single vector meson (see *e.g.*¹²²). Transformations of these common bases to the so-called helicity bases¹²³ can be convenient for the representation of the theoretical results as is *e.g.* discussed in.⁶² They are also beneficial for the determination of form factor parameters from lattice simulations.⁴¹ In order to parametrize the q^2 -dependence of the form factors, one relies on their analytic properties.¹²⁴ Their spectral densities contain potential poles below the crossed-channel pair production threshold; *e.g.* for the $B \rightarrow K$ vector form factor, there is a single pole contribution from the B_s^* meson with mass $M_{B_s^*}^2 < (M_B + M_K)^2$. Moreover, with the onset of the pair production the form factors feature a branch cut extending to $q^2 \rightarrow +\infty$. Following¹²⁴ and later work, these properties can be incorporated into the parametrization of the form factors by virtue of a conformal mapping from q^2 to a variable $z(q^2; t_+, t_0)$. The mapping automatically accounts for the first cross-channel branch cut when equating $t_+ \equiv (M_B + M_K)^2$. A suitable choice of t_0 minimizes the value of $|z|$ in the physical q^2 phase space for semileptonic decays.¹²⁵ The common paradigm^{42,123} to parametrize the form factors is then to first remove the sub-threshold poles through an explicit factor; and second to expand the remaining functions as a Taylor series around $z = 0$. Our present knowledge of the hadronic local matrix elements can be summarised as follows:

- In the case of $B \rightarrow K$ transitions, the form factors are available from both lattice simulations;¹²⁶ Light Cone Sum Rules (LCSRs) with kaon distribution amplitudes;¹²¹ and LCSRs with B -meson Light Cone Distribution Amplitudes (LCDAs).¹²⁷ Either of these results, or combinations thereof have been used in phenomenological applications. A new analysis using LCSRs with B -meson distribution amplitudes is pending.¹²⁸
- The case of $B \rightarrow K^*$ form factors is more complicated since the K^* is not an asymptotic state of QCD. For high-precision analyses, the effects of its finite width have to be taken into account. Lattice results in the narrow-width approximation are available from.¹²⁹ Updated LCSR results for K^* -LCDAs in the narrow-width approximation are provided in,⁴² and a combination of lattice QCD and K^* -LCSR results have been published in.⁴² B -LCSR^{127,130} results do not reach the same level of sophistication as K^* -LCSRs, and updates are expected this year.^{128,131}
- For the case of $B_s \rightarrow \phi$ transitions, the full set of form factors is available from lattice simulations,¹²⁹ and LCSRs with ϕ -LCDAs.⁴²
- The most precise results on $\Lambda_b \rightarrow \Lambda$ transition form factors are available from lattice simulations.¹³² Results on the form factors from LCSRs with Λ -LCDAs are available from.¹³³ For Soft Collinear Effective Theory Sum Rule results from

Λ_b -LCDAs we refer to,¹³⁴ with the complete NLO α_s corrections to the leading Λ_b -LCDAs subsequently published in.¹³⁵

4.2. Hadronic matrix elements of non-local operators

Beside the local semileptonic operators $O_{9,10}$ and their counterparts in NP scenarios, also the operators $O_{1\dots 6,8}$ contribute significantly to the amplitudes. On one hand, the RGE already shows us that roughly 50% of the value of C_9 at the low scale is generated through the RGE mixing of the operators $O_{1c,2c}$ into O_9 . Consequently, this generates a numerically significant scale dependence of C_9 that can only be compensated through the scale dependence of the hadronic matrix elements of these two operators.^e

The latter arise from a *non-local operator*, the time-ordered product with the electromagnetic current $J_{e.m.}$:

$$\mathcal{H}^\mu = i \int d^4x e^{iq \cdot x} \langle H_s(k) | \mathcal{T} \{ J_{e.m.}^\mu(x), \sum_i C_i O_i(0) \} | H_b(p) \rangle, \quad (41)$$

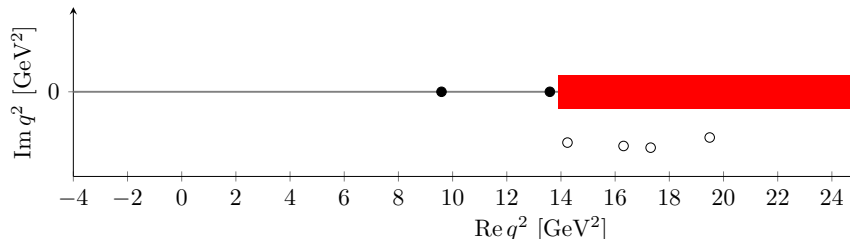
where the sum runs over $i = 1c, 2c, 1u, 2u, 3 \dots 6, 8$. We shorten the following discussion by only considering non-local effects of the operators O_8 and $O_{1c,2c}$, which enter the amplitudes numerically unsuppressed by either small CKM matrix elements or small WC.

To leading power in the heavy quark expansion, the effects due to O_8 can be described in the framework of QCD factorisation (QCDF)^{136,137} as $\mathcal{O}(\alpha_s)$ contributions. When going to subleading power, QCDF breaks down due to endpoint-divergent contributions from terms corresponding to photon emissions from the spectator quark.¹³⁶ This problem can presently only be overcome in the framework of LCSRs.¹³⁸ According to,¹³⁸ the contributions can be written as generalized and complex-valued form factors for meson transitions. The generalized form factors are roughly of the same size as the local matrix elements of O_7 , however, with large phases. They enter the amplitudes with a factor two suppression since $C_7(\mu_b) \simeq 2C_8(\mu_b)$. Additionally, the form factors are further suppressed with increasing q^2 .¹³⁸

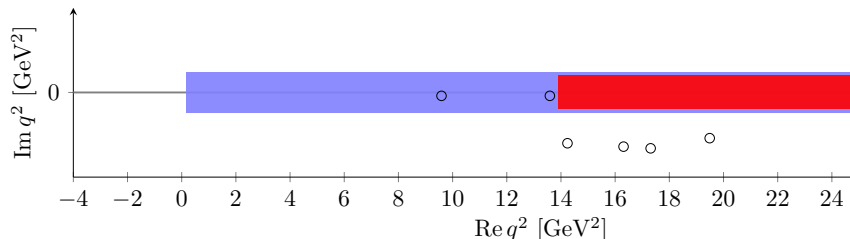
The four-quark operators are both phenomenologically important and conceptually interesting, since they give rise to hadronic decays of the form $H_b \rightarrow H_s V (\rightarrow \gamma^* \rightarrow \ell^+ \ell^-)$. Here V denotes any state with quantum numbers $J^{PC} = 1^{--}$, which can resonantly contribute to the decay rate. A special case here are the $O_{1c,2c}$ contributions, which enter with WCs $C_{1c,2c} = \mathcal{O}(1)$ and at the same level of the

^eIn principle this is also true for the scale dependence of C_7 . However, here the short-distance mixing of the four-quark operators into the electromagnetic operator O_7 are suppressed by α_s .

32 Johannes Albrecht, Stefanie Reichert, Danny van Dyk



(a) Assuming the absence of a branch cut due to light hadrons, with bound states J/ψ and $\psi(2S)$.



(b) In the presence of a branch cut due to light-hadrons, without any bound states.

Fig. 20. Illustration of the analytic structure of the non-local matrix elements of $b\bar{s}c\bar{c}$ operators, in the complex q^2 plane. Bound states are shown as filled circles; resonances are shown as empty circles off the real axis, respectively; and the $D\bar{D}$ branch cut is depicted as the red area extending from $4M_D^2$ to $+\infty$. The blue shaded area depicts the branch cut due to light hadrons (e.g. ϕ , K^+K^-), starting at $4M_\pi^2$. These figures originate from auxiliary materials associated with.¹³⁹

CKM Wolfenstein parameter λ as the short-distance semileptonic contributions. To illustrate the problem, consider the measurements of the branching ratio for the decay $B^0 \rightarrow K^{*0}\mu^+\mu^-$ in the q^2 bin from 1.1 GeV^2 to 6 GeV^2 , which yields $\sim 0.3 \cdot 10^{-7}$, while the resonant hadronic decays $B^0 \rightarrow K^{*0}J/\psi$ and $B^0 \rightarrow K^{*0}\psi(2S)$ yield $\sim 1.3 \cdot 10^{-3}$ and $\sim 0.6 \cdot 10^{-3}$, respectively. These resonant enhancements are denoted as either poles or resonances in the complex q^2 plane in Fig. 20.

Early works on the theoretical description of $b \rightarrow s\ell^+\ell^-$ decays assumed factorisation of the $b \rightarrow s$ quark current from the $c\bar{c}$ loop – usually referred to as *naive factorisation*. A first improvement within the concept of naive factorisation was achieved by Krüger and Sehgal through replacement of the LO quark-loop function by a resonant long-distance contribution extracted from $e^+e^- \rightarrow$ hadrons on the J/ψ and $\psi(2S)$ resonances as well as above the $D\bar{D}$ threshold.¹⁴⁰ The relevant parameters for the description can be inferred from contemporary R ratio measurements,⁸⁸ where

$$R = \frac{\sigma(e^+e^- \rightarrow \text{hadrons})}{\sigma(e^+e^- \rightarrow \mu^+\mu^-)}. \quad (42)$$

A further theoretical improvement was achieved by embedding the four-quark contributions within the frame of QCD factorisation,^{137,141} which holds for $q^2 \ll$

$M_{J/\psi}^2$. The authors were able to show that all contributions to leading power in a combined expansion of local operators in $1/m_b$ and $1/E$, with E the hadron energy in the B rest frame, can be expressed either through local hadronic form factors or convolutions of hard-collinear kernels with B -meson and light-meson LCDAs. Note here that the restriction on the allowed q^2 phase space arises both from the requirements of the power expansion in QCDF, and from estimating a breakdown of the local OPE close to the J/ψ pole. The latter estimate has been questioned more recently in.^{142, 143} By using a Light-Cone OPE (LCOPE), the authors estimate that formally power-suppressed soft contributions become numerically relevant for $q^2 \not\ll 4m_c^2 \simeq 4\text{ GeV}^2$. The leading-power contribution to the LCOPE corresponds to the local OPE such that the QCDF results are completely recovered. At next-to-leading power, corrections to the local OPE from operators involving one soft gluon field can be incorporated. The relevant non-local hadronic matrix elements were estimated from LCSRs. The approximate symmetry of the QCDF results between the two transverse polarization states, arising in the limit of large K^* energy in the B -meson rest frame, can be exploited phenomenologically. A large number of optimised observables have been designed that exhibit a reduced dependence on the local form factors.^{30, 144–146} The now standard basis of optimised observables is $\{P_{1,2,3}, P'_{4,5,6}\}$.⁴⁵

For the phase space with $q^2 \simeq m_b^2$, the four-quark operators can be treated in a local OPE,^{35, 147} commonly referred to as the Low Recoil OPE (LROPE). Due to the universality of the LROPE results for the various K^* and dimuon polarisation states, it gives rise to a rich phenomenology and a set of optimised observables.^{23, 31, 40, 52, 62, 148, 149} In contrast to the theory approaches below the J/ψ , the LROPE results can only be used for sufficiently inclusive q^2 -integrated quantities. The small size of the available phase space in $B \rightarrow K^{(*)}$ decays above the open charm threshold bring into question the LROPE predictions (see *e.g.*¹⁵⁰). Possible relief is an item of active research, and includes: an update to the Krüger/Sehgal model for the resonances including matching onto the LROPE without¹⁵⁰ and with¹⁵¹ the use of endpoint relations among the amplitudes;¹⁴⁹ and explicit models for the violation of quark-hadron duality in rare D decays.¹⁵² Rare D decays might be an interesting laboratory to test our understanding of the long-distance effects, due to their larger hierarchy between long-distance and short-distance effects when compared to the rare B decays.

Very recently, a new approach to the non-local matrix elements below the $\psi(2S)$ has been proposed in a proof-of-concept study.¹³⁹ There the authors parametrize the non-local matrix elements due to $O_{1c,2c}$ in a manner that respects the analytic properties shown in Fig. 20(a). As consequence, theoretical constraints at $q^2 < 0$ and therefore far below any hadronic threshold can be combined with experimental constraints on the non-leptonic decays $B \rightarrow K^* \{J/\psi, \psi(2S)\}$. It remains to be seen how well this approach can be adapted to other exclusive $b \rightarrow s\ell^+\ell^-$ decay modes.

34 Johannes Albrecht, Stefanie Reichert, Danny van Dyk

4.3. Theory predictions in the Standard Model

For the decay $B_s \rightarrow \mu^+ \mu^-$, the presently most precise theoretical predictions include NNLO QCD corrections¹⁵³ and NLO electroweak corrections⁷ at the matching scale, and RGE effects of both QCD and QED in the evolution to the low scale.^{8,9} Non-local power-enhanced QED effects have been taken into consideration for the first time in,⁹⁴ which updates the theory predictions for the observables as follows:

$$\mathcal{B}_{\text{SM}}(B_s^0 \rightarrow \mu^+ \mu^-) = (3.57 \pm 0.17) \cdot 10^{-9}, \quad (43)$$

$$A_{\Delta\Gamma}^{\mu^+ \mu^-} \approx 1 - 1.0 \cdot 10^{-5}, \quad (44)$$

$$C_\lambda \approx \eta_\lambda \cdot 0.6\%, \quad (45)$$

$$S_\lambda \approx -0.1\%. \quad (46)$$

The time-integrated branching ratio \mathcal{B} and the mixing-induced CP asymmetry $A_{\Delta\Gamma}^{\mu^+ \mu^-}$ have been introduced in⁹⁵ and discussed in Section 3.3. The observables C_λ and S_λ are introduced by the time-dependent rate asymmetry¹⁵⁴ Here $\lambda = L, R$ refers to the helicity configuration of the muon pair, and $\eta_{L/R} = \pm 1$. (Note that the above does not yet include the updated results for the B_s meson decay constant by the FNAL/MILC collaborations with a substantially reduced uncertainty.¹¹⁹)

Theory predictions for the semileptonic decays cannot be displayed as succinctly and easily as the ones for the purely leptonic decays. This is due to a large number of choices that need to be made such as the choice of the form factor inputs and parametrisations as well as the treatment of the non-local effects. For $B \rightarrow K^{(*)} \ell \ell$ and $B_s \rightarrow \phi \ell^+ \ell^-$, with either $\ell = e$ or $\ell = \mu$ final states, there are various predictions that differ in these choices.^{14,53,75} However, all of these predictions are mutually compatible at varying degree.

For $\Lambda_b \rightarrow \Lambda \ell^+ \ell^-$, again with $\ell = e, \mu$, there are presently no predictions for $q^2 < M_{J/\psi}^2$ that systematically take non-local effects into account. For predictions at $q^2 > M_{\psi(2S)}^2$ we refer to.¹³²

For the SM predictions of lepton-flavour universality ratios, the treatment of QED effects is very important. For $R_{K^{(*)}}$, this was recently studied in.⁸⁵ For less inclusive observables, such as the angular observables in $B \rightarrow K^* e^+ e^-$, the impact of log-enhanced QED has been discussed in principle in;²⁴ in particular their effects on moments of the angular distribution, and higher moments that do not emerge in the absence of QED effects.

We conclude by referring to existing open source software for the prediction of various observables in exclusive rare (semi-)leptonic B decays. Using both the EOS⁶³ and flavio¹⁵⁵ software, interested parties can gain access to theory predictions within and beyond the SM with the benefit of making their own choices of treatment

for the relevant hadronic effects.

5. Phenomenology and New Physics reach

5.1. Global fits

The large number of measured observables for exclusive $b \rightarrow s\ell^+\ell^-$ transitions has inspired a number of global fits^{14,27} of the WC. These fits rely on constraints of q^2 -integrated observables from the experimental analysis. In addition to these global fits, direct fits of the WC to the observed events have been proposed.^{156–159}

Common to both types of fits are two questions:

- (1) What type of data should be included?
- (2) Which WC should be fitted for, and which can be safely set to their SM values?

The first question has one definite answer: with larger datasets and more complementary data comes greater confidence in the fit results. In addition, the large number of phase space bins allows to perform consistency checks amongst the data. It has been shown that the constraints from individual experiments are in mutual agreement.²⁷ Moreover, removing individual q^2 bins from the analysis allows to extensively check the results for stability against mismodelling of the non-local charm effects. These checks indicate that the results for C_9 obtained from subsets of the q^2 bin are mutually compatible, and no explicit q^2 dependence of the result is found. (see *e.g.*^{14,27}). Beside fitting for only the short-distance information encoded in the WC, it has also been demonstrated that information on the form factors and non-local matrix elements can be inferred alongside the WC.^{12,139,160} By fitting an explicit parametrisation of the non-local matrix elements to data, it was shown that the non-local effects can explain the anomalies, but then fail to explain the q^2 behaviour of the non-local effects as imposed by the dispersion relations and require corrections to the leading-power theory results beyond what is naively expected based on power-counting arguments.^{15,53}

While fits to the mesonic modes $B \rightarrow K^{(*)}\mu^+\mu^-$ and $B_s \rightarrow \phi\mu^+\mu^-$ are by now part of the standard global fits, the inclusion of the baryonic mode $\Lambda_b^0 \rightarrow \Lambda^{(*)}\ell^+\ell^-$ is much more complicated and will require future work to be viable. A first study to that effect concluded that exploitation of the data at low hadronic recoil is possible.⁸⁰ However, the *positive* shift to C_9 which emerges in this study is at odds with the consistent picture of a *negative* shift in all other processes. Moreover, even this positive shift required large duality-violating effects due to non-local charm effects that are incompatible with our present understanding of the LROPE.⁸⁰

The second question has no definite answer: no amount of data, neither from present nor from upcoming experiments, will allow to constrain the entire set of WC simultaneously. The common paradigm is to restrict the fits to the WC of operators of mass dimension six. This is a reasonable restriction, since dimension-eight operators are generically suppressed by factors $M_B^2/M_W^2 \sim 0.5\%$.

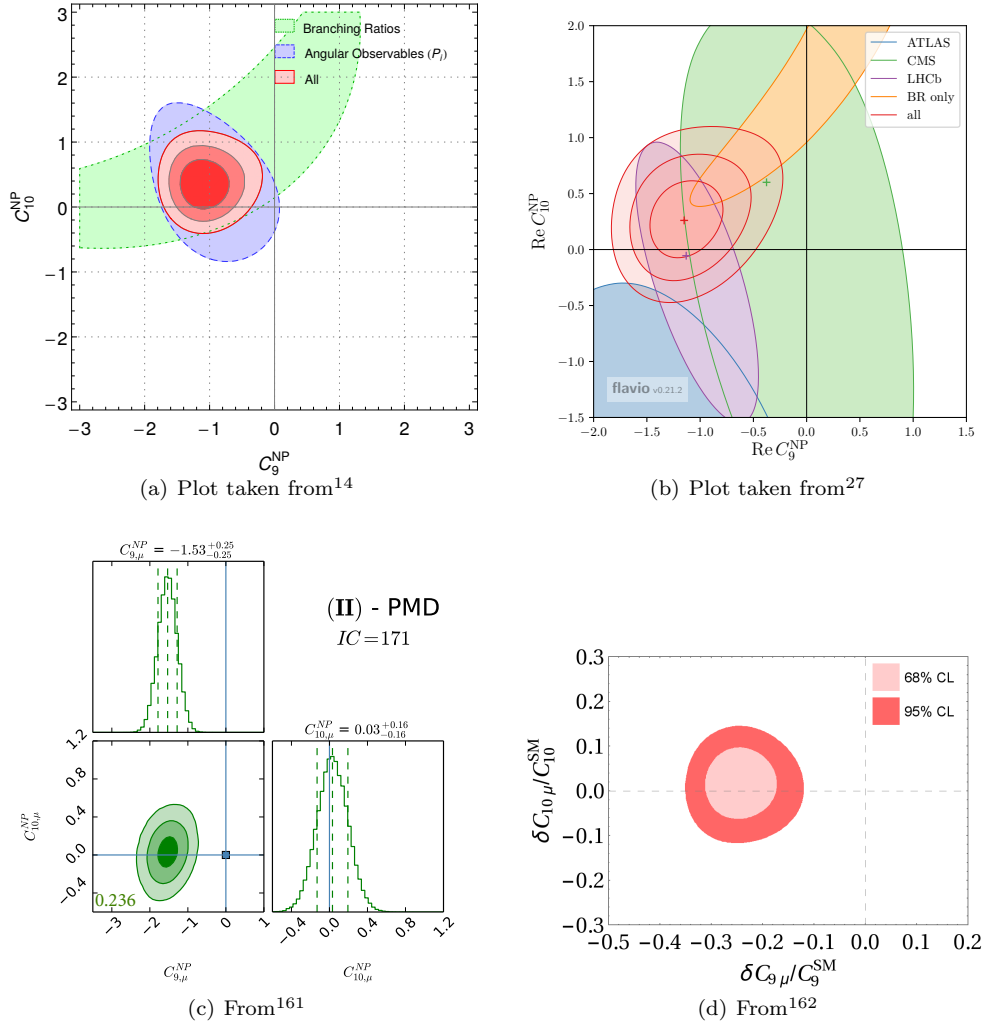


Fig. 21. Plots of the allowed region in the C_9 – C_{10} plane based of four competing analyses. Even though the four analysis use different approaches for the hadronic matrix elements, they all find a substantial tension with respect to the SM value for the parameter C_9 .

The results for fits to $b \rightarrow s\mu^+\mu^-$ data from the various groups as illustrated in Fig. 21 can be summarised as follows:^{14,27,161,162}

- the exclusive data can be fitted reasonably well with the SM ansatz, assuming substantial shifts from theory predictions of the hadronic matrix elements;
- the combination of all $b \rightarrow s\mu^+\mu^-$ data favour a shift to the WC C_9 , which amounts to 25% of its SM value at $\mu \sim 4.2\text{GeV}$;
- there is no clear sign for a q^2 dependence of this shift;

- from a theory perspective, there is presently no irrefutable evidence that this shift is due to NP;

However, in combination with the $b \rightarrow se^+e^-$ data this conclusion changes. Since the measurements of the LFU observables $R_{K^{(*)}}$ cannot be explained by hadronic effects within the SM, all groups find that a NP interpretation of the data is strongly favoured. The shift to C_9 needed to explain the $b \rightarrow s\mu^+\mu^-$ data can simultaneously also explain the signs of LFU violation, if NP are suppressed or absent in $b \rightarrow se^+e^-$ processes. It is therefore now common to distinguish between the Wilson coefficients in both processes according to the lepton flavour, and write $C_9^{(\ell)}$.

Sensitivity studies aimed at the dataset sizes expected from the Belle II experiment and the LHCb Upgrade indicate that the anomalies can exceed a level of 5σ if the present central values remain unchanged;¹⁶³ see Fig. 22 for an illustration. However, it remains to be shown that the shift to $C_9^{(\mu)}$ is indeed a genuine NP effect, and not due to non-local hadronic effects. A promising approach has been recently studied in¹⁵⁹ wherein unbinned fits to the angular distributions of $B^0 \rightarrow K^{*0}\mu^+\mu^-$ and $B^0 \rightarrow K^{*0}e^+e^-$ are carried out simultaneously, yielding accurate and model-independent results for the difference $C_9^{(\mu)} - C_9^{(e)}$. Nevertheless, we emphasise that a better understanding of the non-local hadronic matrix elements is paramount for our understanding of the individual Wilson coefficients $C_9^{(\mu)}$ and $C_9^{(e)}$ and the potential NP models that might give rise to LFU violation.

6. Experimental outlook

The current picture of anomalies in the flavour sector, which have been part of the discussion in this review, promise an interesting future for flavour physics. With the upcoming upgrade of the LHCb detector in 2019-2020 and the start of the Belle II experiment later this year, a confirmation or exclusion of those present-day anomalies is to be expected within the next years. The current available datasets of the LHCb and Belle collaboration correspond to integrated luminosities of 6.7 fb^{-1} at the beginning of 2018 and 0.7 ab^{-1} , respectively. The Belle II experiment is expected to collect 5 ab^{-1} (50 ab^{-1}) by 2020 (2024). With the LHCb detector, an increase to 8 fb^{-1} for this year before the second long shutdown is foreseen. After the scheduled major upgrade of the LHCb detector¹⁶⁴ datasets corresponding to 22 fb^{-1} in 2024 and to 50 fb^{-1} by 2029 will be accumulated.¹⁶⁵

In,¹⁶³ the impact of the future sensitivities at those well-defined milestones in 2020, 2024 and 2029 are estimated and their impact on global fits to the Wilson Coefficients is discussed. An illustration of the impact of future sensitivities of the Belle II and LHCb experiments and their complementarity is shown in Fig. 22. As can be seen from Fig. 22, the primed semileptonic operators as well as the electromagnetic dipole operators are currently consistent with the SM hypothesis. However, the current measurements exhibit a tension from the SM in C_9 (see Section 5.1), which

38 *Johannes Albrecht, Stefanie Reichert, Danny van Dyk*

seems to be lower than the SM prediction. No discrepancy to the SM prediction is observed for C_{10} .

It is expected that the sensitivities of the upgraded LHCb experiment and the Belle II detector will allow to either exclude or confirm the currently observed anomalies within the next years. If the current anomalies in $R(K)$ and $R(K^*)$ stay at their respective central values, then LHCb should be able to measure $R(K)$ and $R(K^*)$ with a significance exceeding 5σ already with a dataset corresponding to 8 fb^{-1} . The Belle II collaboration will reach the required sensitivities with a dataset of 5 ab^{-1} foreseen to be collected in 2020. Due to the available statistics and improvements to the detector, the origin of the anomalies in the flavour sector is expected to be discovered within the next years and will allow us to gain insight about potential physics beyond the SM.

Acknowledgments

J. A. gratefully acknowledges support of the Deutsche Forschungsgemeinschaft (DFG, Emmy Noether programme: AL 1639/1-1) and of the European Research Council (ERC Starting Grant: PRECISION 714536).

D. v. D. gratefully acknowledges support of the Deutsche Forschungsgemeinschaft (DFG) within the Emmy Noether programme under contract DY 130/1-1 and through the DFG Collaborative Research Center 110 “Symmetries and the Emergence of Structure in QCD”.

The authors thank Yasmine Amhis and Javier Virto for proof-reading the manuscript.

References

1. G. Buchalla, A. J. Buras and M. E. Lautenbacher, *Rev. Mod. Phys.* **68**, 1125 (1996), [arXiv:hep-ph/9512380 \[hep-ph\]](#), doi:10.1103/RevModPhys.68.1125.
2. C. Bobeth, M. Misiak and J. Urban, *Nucl. Phys.* **B574**, 291 (2000), [arXiv:hep-ph/9910220 \[hep-ph\]](#), doi:10.1016/S0550-3213(00)00007-9.
3. M. Misiak and M. Steinhauser, *Nucl. Phys.* **B683**, 277 (2004), [arXiv:hep-ph/0401041 \[hep-ph\]](#), doi:10.1016/j.nuclphysb.2004.02.006.
4. M. Gorbahn and U. Haisch, *Nucl. Phys.* **B713**, 291 (2005), [arXiv:hep-ph/0411071 \[hep-ph\]](#), doi:10.1016/j.nuclphysb.2005.01.047.
5. M. Gorbahn, U. Haisch and M. Misiak, *Phys. Rev. Lett.* **95**, 102004 (2005), [arXiv:hep-ph/0504194 \[hep-ph\]](#), doi:10.1103/PhysRevLett.95.102004.
6. M. Czakon, U. Haisch and M. Misiak, *JHEP* **03**, 008 (2007), [arXiv:hep-ph/0612329 \[hep-ph\]](#), doi:10.1088/1126-6708/2007/03/008.
7. C. Bobeth, M. Gorbahn and E. Stamou, *Phys. Rev.* **D89**, 034023 (2014), [arXiv:1311.1348 \[hep-ph\]](#), doi:10.1103/PhysRevD.89.034023.
8. C. Bobeth, P. Gambino, M. Gorbahn and U. Haisch, *JHEP* **04**, 071 (2004), [arXiv:hep-ph/0312090 \[hep-ph\]](#), doi:10.1088/1126-6708/2004/04/071.

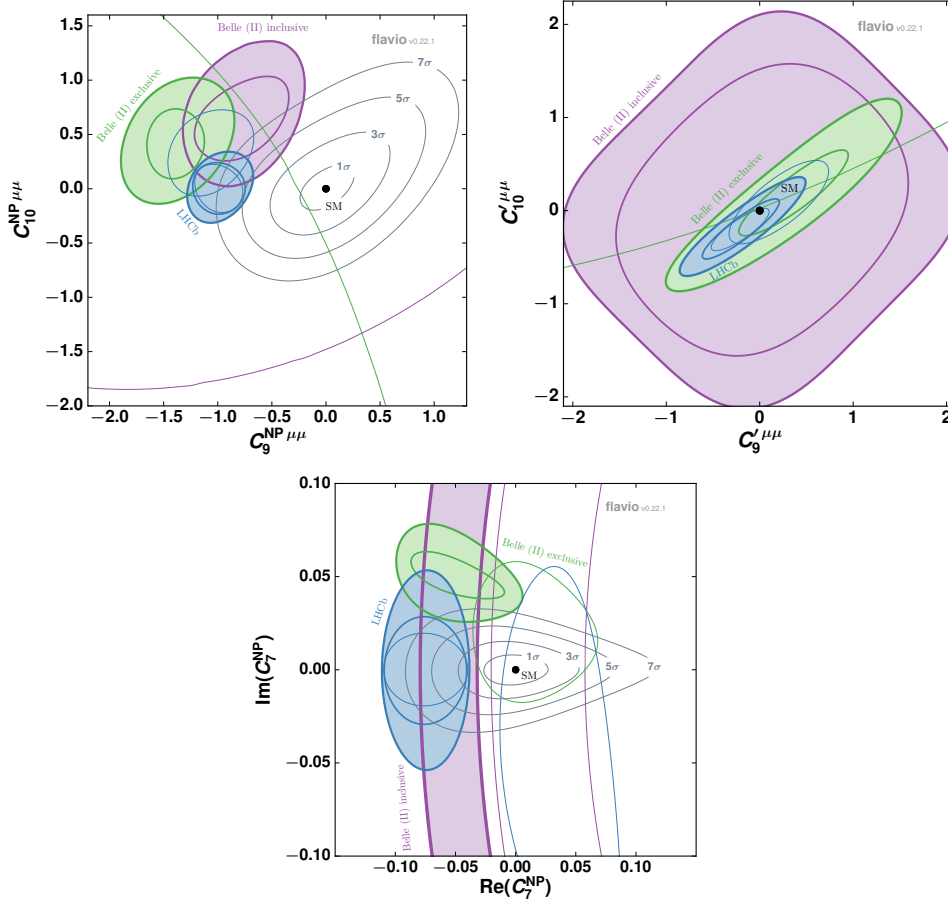


Fig. 22. Two-dimensional scans of the new physics contribution to $C_9^{\text{NP}\mu\mu}$ versus $C_{10}^{\text{NP}\mu\mu}$ (top left), $C_9^{\mu\mu}$ versus $C_{10}^{\mu\mu}$ (top right) and $\text{Re}(C_7^{\text{NP}})$ versus $\text{Im}(C_7^{\text{NP}})$ (bottom). Displayed are the current average (not filled) as well as the extrapolations to future sensitivities (filled) of LHCb at 8 fb^{-1} , 22 fb^{-1} and 50 fb^{-1} (exclusive decays) and of Belle II at 5 ab^{-1} and 50 ab^{-1} (both inclusive and exclusive decays) assuming different NP models for the three classes of measurements to aid visibility. The SM prediction (black dot) with the 1σ , 3σ , 5σ and 7σ exclusion contours with a combined sensitivity of LHCb's 50 fb^{-1} and Belle II's 50 ab^{-1} datasets is indicated in light grey. As the primed operators show no tensions with respect to the SM, no SM exclusions are provided. Figures from.¹⁶³

9. T. Huber, E. Lunghi, M. Misiak and D. Wyler, *Nucl. Phys.* **B740**, 105 (2006), [arXiv:hep-ph/0512066 \[hep-ph\]](#), doi:10.1016/j.nuclphysb.2006.01.037.
10. A. Ali, G. F. Giudice and T. Mannel, *Z. Phys.* **C67**, 417 (1995), [arXiv:hep-ph/9408213 \[hep-ph\]](#), doi:10.1007/BF01624585.
11. J. Aebischer, M. Fael, C. Greub and J. Virto, *JHEP* **09**, 158 (2017), [arXiv:1704.06639 \[hep-ph\]](#), doi:10.1007/JHEP09(2017)158.
12. F. Beaujean, C. Bobeth and D. van Dyk, *Eur. Phys. J.* **C74**, 2897 (2014), [arXiv:1310.2478 \[hep-ph\]](#), doi:10.1140/epjc/s10052-014-2897-0,10.1140/

40 *Johannes Albrecht, Stefanie Reichert, Danny van Dyk*

- epjc/s10052-014-3179-6, [Erratum: Eur. Phys. J.C74,3179(2014)].
13. F. Beaujean, C. Bobeth and S. Jahn, *Eur. Phys. J.* **C75**, 456 (2015), [arXiv:1508.01526 \[hep-ph\]](#), doi:10.1140/epjc/s10052-015-3676-2.
 14. S. Descotes-Genon, L. Hofer, J. Matias and J. Virto, *JHEP* **06**, 092 (2016), [arXiv:1510.04239 \[hep-ph\]](#), doi:10.1007/JHEP06(2016)092.
 15. T. Hurth, F. Mahmoudi and S. Neshatpour, *Nucl. Phys.* **B909**, 737 (2016), [arXiv:1603.00865 \[hep-ph\]](#), doi:10.1016/j.nuclphysb.2016.05.022.
 16. R. Alonso, B. Grinstein and J. Martin Camalich, *Phys. Rev. Lett.* **113**, 241802 (2014), [arXiv:1407.7044 \[hep-ph\]](#), doi:10.1103/PhysRevLett.113.241802.
 17. O. Catà and M. Jung, *Phys. Rev.* **D92**, 055018 (2015), [arXiv:1505.05804 \[hep-ph\]](#), doi:10.1103/PhysRevD.92.055018.
 18. W. Buchmuller and D. Wyler, *Nucl. Phys.* **B268**, 621 (1986), doi:10.1016/0550-3213(86)90262-2.
 19. J. Aebischer, A. Crivellin, M. Fael and C. Greub, *JHEP* **05**, 037 (2016), [arXiv:1512.02830 \[hep-ph\]](#), doi:10.1007/JHEP05(2016)037.
 20. A. Celis, J. Fuentes-Martin, A. Vicente and J. Virto, *Eur. Phys. J.* **C77**, 405 (2017), [arXiv:1704.04504 \[hep-ph\]](#), doi:10.1140/epjc/s10052-017-4967-6.
 21. J. Aebischer *et al.* (2017), [arXiv:1712.05298 \[hep-ph\]](#).
 22. J. Aebischer, J. Kumar and D. M. Straub (2018), [arXiv:1804.05033 \[hep-ph\]](#).
 23. C. Bobeth, G. Hiller and D. van Dyk, *Phys. Rev.* **D87**, 034016 (2013), [arXiv:1212.2321 \[hep-ph\]](#), doi:10.1103/PhysRevD.87.034016.
 24. J. Gratex, M. Hopfer and R. Zwicky, *Phys. Rev.* **D93**, 054008 (2016), [arXiv:1506.03970 \[hep-ph\]](#), doi:10.1103/PhysRevD.93.054008.
 25. D. Das (2018), [arXiv:1804.08527 \[hep-ph\]](#).
 26. S. Descotes-Genon, J. Matias and J. Virto, *Phys. Rev.* **D88**, 074002 (2013), [arXiv:1307.5683 \[hep-ph\]](#), doi:10.1103/PhysRevD.88.074002.
 27. W. Altmannshofer, C. Niehoff, P. Stangl and D. M. Straub, *Eur. Phys. J.* **C77**, 377 (2017), [arXiv:1703.09189 \[hep-ph\]](#), doi:10.1140/epjc/s10052-017-4952-0.
 28. LHCb Collaboration (R. Aaij *et al.*), *JHEP* **06**, 133 (2014), [arXiv:1403.8044 \[hep-ex\]](#), doi:10.1007/JHEP06(2014)133.
 29. LHCb Collaboration (R. Aaij *et al.*), *JHEP* **09**, 177 (2014), [arXiv:1408.0978 \[hep-ex\]](#), doi:10.1007/JHEP09(2014)177.
 30. W. Altmannshofer, P. Ball, A. Bharucha, A. J. Buras, D. M. Straub and M. Wick, *JHEP* **01**, 019 (2009), [arXiv:0811.1214 \[hep-ph\]](#), doi:10.1088/1126-6708/2009/01/019.
 31. C. Bobeth, G. Hiller, D. van Dyk and C. Wacker, *JHEP* **01**, 107 (2012), [arXiv:1111.2558 \[hep-ph\]](#), doi:10.1007/JHEP01(2012)107.
 32. C. Bobeth, G. Hiller and G. Piranishvili, *JHEP* **12**, 040 (2007), [arXiv:0709.4174 \[hep-ph\]](#), doi:10.1088/1126-6708/2007/12/040.
 33. LHCb Collaboration (R. Aaij *et al.*), *JHEP* **05**, 082 (2014), [arXiv:1403.8045 \[hep-ex\]](#), doi:10.1007/JHEP05(2014)082.
 34. LHCb Collaboration (R. Aaij *et al.*), *Phys. Rev. Lett.* **111**, 112003 (2013), [arXiv:1307.7595 \[hep-ex\]](#), doi:10.1103/PhysRevLett.111.112003.
 35. M. Beylich, G. Buchalla and T. Feldmann, *Eur. Phys. J.* **C71**, 1635 (2011), [arXiv:1101.5118 \[hep-ph\]](#), doi:10.1140/epjc/s10052-011-1635-0.
 36. LHCb Collaboration (R. Aaij *et al.*), *Eur. Phys. J.* **C77**, 161 (2017), [arXiv:1612.06764 \[hep-ex\]](#), doi:10.1140/epjc/s10052-017-4703-2.
 37. LHCb Collaboration (R. Aaij *et al.*), *JHEP* **08**, 131 (2013), [arXiv:1304.6325 \[hep-ex\]](#), doi:10.1007/JHEP08(2013)131.
 38. LHCb

- Collaboration (R. Aaij *et al.*), *JHEP* **11**, 047 (2016), [arXiv:1606.04731 \[hep-ex\]](#), doi:10.1007/JHEP11(2016)047, 10.1007/JHEP04(2017)142, [Erratum: *JHEP* **04**, 142 (2017)].
39. CMS Collaboration (V. Khachatryan *et al.*), *Phys. Lett.* **B753**, 424 (2016), [arXiv:1507.08126 \[hep-ex\]](#), doi:10.1016/j.physletb.2015.12.020.
 40. C. Bobeth, G. Hiller and D. van Dyk, *JHEP* **07**, 067 (2011), [arXiv:1105.0376 \[hep-ph\]](#), doi:10.1007/JHEP07(2011)067.
 41. R. R. Horgan, Z. Liu, S. Meinel and M. Wingate, *Phys. Rev.* **D89**, 094501 (2014), [arXiv:1310.3722 \[hep-lat\]](#), doi:10.1103/PhysRevD.89.094501.
 42. A. Bharucha, D. M. Straub and R. Zwicky, *JHEP* **08**, 098 (2016), [arXiv:1503.05534 \[hep-ph\]](#), doi:10.1007/JHEP08(2016)098.
 43. F. Kruger, L. M. Sehgal, N. Sinha and R. Sinha, *Phys. Rev.* **D61**, 114028 (2000), [arXiv:hep-ph/9907386 \[hep-ph\]](#), doi:10.1103/PhysRevD.61.114028, 10.1103/PhysRevD.63.019901, [Erratum: *Phys. Rev.* **D63**, 019901 (2001)].
 44. F. Kruger and J. Matias, *Phys. Rev.* **D71**, 094009 (2005), [arXiv:hep-ph/0502060 \[hep-ph\]](#), doi:10.1103/PhysRevD.71.094009.
 45. S. Descotes-Genon, J. Matias, M. Ramon and J. Virto, *JHEP* **01**, 048 (2013), [arXiv:1207.2753 \[hep-ph\]](#), doi:10.1007/JHEP01(2013)048.
 46. J. Matias, *Phys. Rev.* **D86**, 094024 (2012), [arXiv:1209.1525 \[hep-ph\]](#), doi:10.1103/PhysRevD.86.094024.
 47. J. Matias, F. Mescia, M. Ramon and J. Virto, *JHEP* **04**, 104 (2012), [arXiv:1202.4266 \[hep-ph\]](#), doi:10.1007/JHEP04(2012)104.
 48. CMS Collaboration (A. M. Sirunyan *et al.*), *Phys. Lett.* **B781**, 517 (2018), [arXiv:1710.02846 \[hep-ex\]](#), doi:10.1016/j.physletb.2018.04.030.
 49. LHCb Collaboration (R. Aaij *et al.*), *Phys. Rev. Lett.* **111**, 191801 (2013), [arXiv:1308.1707 \[hep-ex\]](#), doi:10.1103/PhysRevLett.111.191801.
 50. LHCb Collaboration (R. Aaij *et al.*), *JHEP* **02**, 104 (2016), [arXiv:1512.04442 \[hep-ex\]](#), doi:10.1007/JHEP02(2016)104.
 51. Belle Collaboration (S. Wehle *et al.*), *Phys. Rev. Lett.* **118**, 111801 (2017), [arXiv:1612.05014 \[hep-ex\]](#), doi:10.1103/PhysRevLett.118.111801.
 52. S. Descotes-Genon, T. Hurth, J. Matias and J. Virto, *JHEP* **05**, 137 (2013), [arXiv:1303.5794 \[hep-ph\]](#), doi:10.1007/JHEP05(2013)137.
 53. M. Ciuchini, M. Fedele, E. Franco, S. Mishima, A. Paul, L. Silvestrini and M. Valli, *JHEP* **06**, 116 (2016), [arXiv:1512.07157 \[hep-ph\]](#), doi:10.1007/JHEP06(2016)116.
 54. M. Ciuchini, M. Fedele, E. Franco, S. Mishima, A. Paul, L. Silvestrini and M. Valli, *PoS ICHEP2016*, 584 (2016), [arXiv:1611.04338 \[hep-ph\]](#).
 55. R. R. Horgan, Z. Liu, S. Meinel and M. Wingate, *PoS LATTICE2014*, 372 (2015), [arXiv:1501.00367 \[hep-lat\]](#).
 56. B. Capdevila, S. Descotes-Genon, J. Matias and J. Virto, *JHEP* **10**, 075 (2016), [arXiv:1605.03156 \[hep-ph\]](#), doi:10.1007/JHEP10(2016)075.
 57. ATLAS Collaboration (M. Aaboud *et al.*) (2018), [arXiv:1805.04000 \[hep-ex\]](#).
 58. S. Jäger and J. Martin Camalich, *JHEP* **05**, 043 (2013), [arXiv:1212.2263 \[hep-ph\]](#), doi:10.1007/JHEP05(2013)043.
 59. S. Jäger and J. Martin Camalich, *Phys. Rev.* **D93**, 014028 (2016), [arXiv:1412.3183 \[hep-ph\]](#), doi:10.1103/PhysRevD.93.014028.
 60. F. Beaujean, M. Chrzaszcz, N. Serra and D. van Dyk, *Phys. Rev.* **D91**, 114012 (2015), [arXiv:1503.04100 \[hep-ex\]](#), doi:10.1103/PhysRevD.91.114012.
 61. S. Descotes-Genon, L. Hofer, J. Matias and J. Virto, *JHEP* **12**, 125 (2014), [arXiv:1407.8526 \[hep-ph\]](#), doi:10.1007/JHEP12(2014)125.

42 Johannes Albrecht, Stefanie Reichert, Danny van Dyk

62. C. Bobeth, G. Hiller and D. van Dyk, *JHEP* **07**, 098 (2010), [arXiv:1006.5013 \[hep-ph\]](#), doi:10.1007/JHEP07(2010)098.
63. D. van Dyk *et al.*, EOS — A HEP program for Flavor Observables <https://eos.github.io>, (2018).
64. BaBar Collaboration (J. P. Lees *et al.*), *Phys. Rev.* **D93**, 052015 (2016), [arXiv:1508.07960 \[hep-ex\]](#), doi:10.1103/PhysRevD.93.052015.
65. Belle Collaboration (J. T. Wei *et al.*), *Phys. Rev. Lett.* **103**, 171801 (2009), [arXiv:0904.0770 \[hep-ex\]](#), doi:10.1103/PhysRevLett.103.171801.
66. CDF Collaboration (T. Aaltonen *et al.*), *Phys. Rev. Lett.* **108**, 081807 (2012), [arXiv:1108.0695 \[hep-ex\]](#), doi:10.1103/PhysRevLett.108.081807.
67. CMS Collaboration (S. Chatrchyan *et al.*), *Phys. Lett.* **B727**, 77 (2013), [arXiv:1308.3409 \[hep-ex\]](#), doi:10.1016/j.physletb.2013.10.017.
68. ATLAS Collaboration, (G. Aad *et al.*), Angular Analysis of $B_d \rightarrow K^{*0} \mu^+ \mu^-$ with the ATLAS Experiment (2013), ATLAS-CONF-2013-038.
69. LHCb Collaboration (R. Aaij *et al.*), *JHEP* **05**, 159 (2013), [arXiv:1304.3035 \[hep-ex\]](#), doi:10.1007/JHEP05(2013)159.
70. LHCb Collaboration (R. Aaij *et al.*), *JHEP* **04**, 064 (2015), [arXiv:1501.03038 \[hep-ex\]](#), doi:10.1007/JHEP04(2015)064.
71. LHCb Collaboration (R. Aaij *et al.*), *JHEP* **10**, 064 (2014), [arXiv:1408.1137 \[hep-ex\]](#), doi:10.1007/JHEP10(2014)064.
72. LHCb Collaboration (R. Aaij *et al.*), *JHEP* **12**, 065 (2016), [arXiv:1609.04736 \[hep-ex\]](#), doi:10.1007/JHEP12(2016)065.
73. LHCb Collaboration (R. Aaij *et al.*), *JHEP* **09**, 179 (2015), [arXiv:1506.08777 \[hep-ex\]](#), doi:10.1007/JHEP09(2015)179.
74. LHCb Collaboration (R. Aaij *et al.*), *JHEP* **07**, 084 (2013), [arXiv:1305.2168 \[hep-ex\]](#), doi:10.1007/JHEP07(2013)084.
75. W. Altmannshofer and D. M. Straub, *Eur. Phys. J.* **C75**, 382 (2015), [arXiv:1411.3161 \[hep-ph\]](#), doi:10.1140/epjc/s10052-015-3602-7.
76. BaBar Collaboration (J. P. Lees *et al.*), *Phys. Rev. Lett.* **112**, 211802 (2014), [arXiv:1312.5364 \[hep-ex\]](#), doi:10.1103/PhysRevLett.112.211802.
77. Belle Collaboration (Y. Sato *et al.*), *Phys. Rev.* **D93**, 032008 (2016), [arXiv:1402.7134 \[hep-ex\]](#), doi:10.1103/PhysRevD.93.059901,10.1103/PhysRevD.93.032008, [Addendum: *Phys. Rev.* **D93**, 059901 (2016)].
78. P. Böer, T. Feldmann and D. van Dyk, *JHEP* **01**, 155 (2015), [arXiv:1410.2115 \[hep-ph\]](#), doi:10.1007/JHEP01(2015)155.
79. LHCb Collaboration (R. Aaij *et al.*), *JHEP* **06**, 115 (2015), [arXiv:1503.07138 \[hep-ex\]](#), doi:10.1007/JHEP06(2015)115.
80. S. Meinel and D. van Dyk, *Phys. Rev.* **D94**, 013007 (2016), [arXiv:1603.02974 \[hep-ph\]](#), doi:10.1103/PhysRevD.94.013007.
81. S. Meinel, *PoS LATTICE2013*, 024 (2014), [arXiv:1401.2685 \[hep-lat\]](#).
82. D. Das, *Eur. Phys. J.* **C78**, 230 (2018), [arXiv:1802.09404 \[hep-ph\]](#), doi:10.1140/epjc/s10052-018-5731-2.
83. T. Blake and M. Kreps, *JHEP* **11**, 138 (2017), [arXiv:1710.00746 \[hep-ph\]](#), doi:10.1007/JHEP11(2017)138.
84. G. Hiller and F. Kruger, *Phys. Rev.* **D69**, 074020 (2004), [arXiv:hep-ph/0310219 \[hep-ph\]](#), doi:10.1103/PhysRevD.69.074020.
85. M. Bordone, G. Isidori and A. Pattori, *Eur. Phys. J.* **C76**, 440 (2016), [arXiv:1605.07633 \[hep-ph\]](#), doi:10.1140/epjc/s10052-016-4274-7.
86. LHCb Collaboration (R. Aaij *et al.*), *Phys. Rev. Lett.* **113**, 151601 (2014), [arXiv:1406.6482 \[hep-ex\]](#), doi:10.1103/PhysRevLett.113.151601.

87. LHCb Collaboration (R. Aaij *et al.*), *JHEP* **08**, 055 (2017), [arXiv:1705.05802 \[hep-ex\]](#), doi:10.1007/JHEP08(2017)055.
88. Particle Data Group Collaboration (C. Patrignani *et al.*), *Chin. Phys.* **C40**, 100001 (2016), doi:10.1088/1674-1137/40/10/100001.
89. BaBar Collaboration (J. P. Lees *et al.*), *Phys. Rev.* **D86**, 032012 (2012), [arXiv:1204.3933 \[hep-ex\]](#), doi:10.1103/PhysRevD.86.032012.
90. G. D'Ambrosio, G. F. Giudice, G. Isidori and A. Strumia, *Nucl. Phys.* **B645**, 155 (2002), [arXiv:hep-ph/0207036 \[hep-ph\]](#), doi:10.1016/S0550-3213(02)00836-2.
91. LHCb Collaboration (R. Aaij *et al.*), *JHEP* **10**, 034 (2015), [arXiv:1509.00414 \[hep-ex\]](#), doi:10.1007/JHEP10(2015)034.
92. LHCb Collaboration (R. Aaij *et al.*), *Phys. Lett.* **B743**, 46 (2015), [arXiv:1412.6433 \[hep-ex\]](#), doi:10.1016/j.physletb.2015.02.010.
93. LHCb Collaboration (R. Aaij *et al.*) (2018), [arXiv:1804.07167 \[hep-ex\]](#).
94. M. Beneke, C. Bobeth and R. Szafron, *Phys. Rev. Lett.* **120**, 011801 (2018), [arXiv:1708.09152 \[hep-ph\]](#), doi:10.1103/PhysRevLett.120.011801.
95. K. De Bruyn, R. Fleischer, R. Knegjens, P. Koppenburg, M. Merk and N. Tuning, *Phys. Rev.* **D86**, 014027 (2012), [arXiv:1204.1735 \[hep-ph\]](#), doi:10.1103/PhysRevD.86.014027.
96. T. P. Cheng and M. Sher, *Phys. Rev.* **D35**, 3484 (1987), doi:10.1103/PhysRevD.35.3484.
97. J. L. Diaz-Cruz, R. Noriega-Papaqui and A. Rosado, *Phys. Rev.* **D69**, 095002 (2004), [arXiv:hep-ph/0401194 \[hep-ph\]](#), doi:10.1103/PhysRevD.69.095002.
98. LHCb Collaboration (R. Aaij *et al.*), *Phys. Rev. Lett.* **111**, 101805 (2013), [arXiv:1307.5024 \[hep-ex\]](#), doi:10.1103/PhysRevLett.111.101805.
99. LHCb, CMS Collaboration (V. Khachatryan *et al.*), *Nature* **522**, 68 (2015), [arXiv:1411.4413 \[hep-ex\]](#), doi:10.1038/nature14474.
100. ATLAS Collaboration (M. Aaboud *et al.*), *Eur. Phys. J.* **C76**, 513 (2016), [arXiv:1604.04263 \[hep-ex\]](#), doi:10.1140/epjc/s10052-016-4338-8.
101. LHCb Collaboration (R. Aaij *et al.*), *Phys. Rev. Lett.* **118**, 191801 (2017), [arXiv:1703.05747 \[hep-ex\]](#), doi:10.1103/PhysRevLett.118.191801.
102. F. Dettori, LHCb-TALK-2017-147 <https://cds.cern.ch/record/2268280>, (2017).
103. R. Fleischer, R. Jaarsma and G. Tetlalmatzi-Xolocotzi, *JHEP* **05**, 156 (2017), [arXiv:1703.10160 \[hep-ph\]](#), doi:10.1007/JHEP05(2017)156.
104. J. M. Cline, *Phys. Rev.* **D93**, 075017 (2016), [arXiv:1512.02210 \[hep-ph\]](#), doi:10.1103/PhysRevD.93.075017.
105. D. Bečirević, S. Fajfer, N. Košnik and O. Sumensari, *Phys. Rev.* **D94**, 115021 (2016), [arXiv:1608.08501 \[hep-ph\]](#), doi:10.1103/PhysRevD.94.115021.
106. CDF Collaboration (T. Aaltonen *et al.*), *Phys. Rev. Lett.* **102**, 201801 (2009), [arXiv:0901.3803 \[hep-ex\]](#), doi:10.1103/PhysRevLett.102.201801.
107. C. Bobeth, M. Gorbahn, T. Hermann, M. Misiak, E. Stamou and M. Steinhauser, *Phys. Rev. Lett.* **112**, 101801 (2014), [arXiv:1311.0903 \[hep-ph\]](#), doi:10.1103/PhysRevLett.112.101801.
108. LHCb Collaboration (R. Aaij *et al.*), *Phys. Rev. Lett.* **118**, 251802 (2017), [arXiv:1703.02508 \[hep-ex\]](#), doi:10.1103/PhysRevLett.118.251802.
109. T. Blake, T. Gershon and G. Hiller, *Ann. Rev. Nucl. Part. Sci.* **65**, 113 (2015), [arXiv:1501.03309 \[hep-ex\]](#), doi:10.1146/annurev-nucl-102014-022231.
110. Belle Collaboration (T. Horiguchi *et al.*), *Phys. Rev. Lett.* **119**, 191802 (2017), [arXiv:1707.00394 \[hep-ex\]](#), doi:10.1103/PhysRevLett.119.191802.
111. M. Jung, *Phys. Lett.* **B753**, 187 (2016), [arXiv:1510.03423 \[hep-ph\]](#), doi:10.1016/j.physletb.2015.12.024.

44 Johannes Albrecht, Stefanie Reichert, Danny van Dyk

112. Belle Collaboration (D. Dutta *et al.*), *Phys. Rev.* **D91**, 011101 (2015), [arXiv:1411.7771 \[hep-ex\]](#), doi:10.1103/PhysRevD.91.011101.
113. LHCb Collaboration (R. Aaij *et al.*), *Nucl. Phys.* **B867**, 1 (2013), [arXiv:1209.0313 \[hep-ex\]](#), doi:10.1016/j.nuclphysb.2012.09.013.
114. LHCb Collaboration (R. Aaij *et al.*), *Phys. Rev. Lett.* **118**, 021801 (2017), [arXiv:1609.02032 \[hep-ex\]](#), doi:10.1103/PhysRevLett.118.021801,10.1103/PhysRevLett.118.109901, [Addendum: *Phys. Rev. Lett.* **118**, 109901 (2017)].
115. Belle Collaboration (Z. King *et al.*), *Phys. Rev.* **D93**, 111101 (2016), [arXiv:1603.06546 \[hep-ex\]](#), doi:10.1103/PhysRevD.93.111101.
116. S. Aoki *et al.*, *Eur. Phys. J.* **C77**, 112 (2017), [arXiv:1607.00299 \[hep-lat\]](#), doi:10.1140/epjc/s10052-016-4509-7.
117. N. Carrasco *et al.*, *PoS LATTICE2013*, 313 (2014), [arXiv:1311.2837 \[hep-lat\]](#).
118. HPQCD Collaboration (R. J. Dowdall, C. T. H. Davies, R. R. Horgan, C. J. Monahan and J. Shigemitsu), *Phys. Rev. Lett.* **110**, 222003 (2013), [arXiv:1302.2644 \[hep-lat\]](#), doi:10.1103/PhysRevLett.110.222003.
119. A. Bazavov *et al.* (2017), [arXiv:1712.09262 \[hep-lat\]](#).
120. P. Gelhausen, A. Khodjamirian, A. A. Pivovarov and D. Rosenthal, *Eur. Phys. J.* **C74**, 2979 (2014), [arXiv:1404.5891 \[hep-ph\]](#), doi:10.1140/epjc/s10052-014-2979-z.
121. P. Ball and R. Zwicky, *Phys. Rev.* **D71**, 014015 (2005), [arXiv:hep-ph/0406232 \[hep-ph\]](#), doi:10.1103/PhysRevD.71.014015.
122. P. Ball and R. Zwicky, *Phys. Rev.* **D71**, 014029 (2005), [arXiv:hep-ph/0412079 \[hep-ph\]](#), doi:10.1103/PhysRevD.71.014029.
123. A. Bharucha, T. Feldmann and M. Wick, *JHEP* **09**, 090 (2010), [arXiv:1004.3249 \[hep-ph\]](#), doi:10.1007/JHEP09(2010)090.
124. C. G. Boyd, B. Grinstein and R. F. Lebed, *Nucl. Phys.* **B461**, 493 (1996), [arXiv:hep-ph/9508211 \[hep-ph\]](#), doi:10.1016/0550-3213(95)00653-2.
125. C. Bourrely, I. Caprini and L. Lellouch, *Phys. Rev.* **D79**, 013008 (2009), [arXiv:0807.2722 \[hep-ph\]](#), doi:10.1103/PhysRevD.82.099902,10.1103/PhysRevD.79.013008, [Erratum: *Phys. Rev.* **D82**, 099902 (2010)].
126. HPQCD Collaboration (C. Bouchard, G. P. Lepage, C. Monahan, H. Na and J. Shigemitsu), *Phys. Rev.* **D88**, 054509 (2013), [arXiv:1306.2384 \[hep-lat\]](#), doi:10.1103/PhysRevD.88.079901,10.1103/PhysRevD.88.054509, [Erratum: *Phys. Rev.* **D88**, 079901 (2013)].
127. A. Khodjamirian, T. Mannel and N. Offen, *Phys. Rev.* **D75**, 054013 (2007), [arXiv:hep-ph/0611193 \[hep-ph\]](#), doi:10.1103/PhysRevD.75.054013.
128. N. Gubernari, A. Kokulu and D. van Dyk, in preparation (2018).
129. R. R. Horgan, Z. Liu, S. Meinel and M. Wingate, *Phys. Rev. Lett.* **112**, 212003 (2014), [arXiv:1310.3887 \[hep-ph\]](#), doi:10.1103/PhysRevLett.112.212003.
130. S. Cheng, A. Khodjamirian and J. Virto, *JHEP* **05**, 157 (2017), [arXiv:1701.01633 \[hep-ph\]](#), doi:10.1007/JHEP05(2017)157.
131. S. Descotes-Genone, A. Khodjamirian, J. Virto and K. Vos, in preparation (2018).
132. W. Detmold and S. Meinel, *Phys. Rev.* **D93**, 074501 (2016), [arXiv:1602.01399 \[hep-lat\]](#), doi:10.1103/PhysRevD.93.074501.
133. T. Mannel and Y.-M. Wang, *JHEP* **12**, 067 (2011), [arXiv:1111.1849 \[hep-ph\]](#), doi:10.1007/JHEP12(2011)067.
134. T. Feldmann and M. W. Y. Yip, *Phys. Rev.* **D85**, 014035 (2012), [arXiv:1111.1844 \[hep-ph\]](#), doi:10.1103/PhysRevD.85.014035,10.1103/PhysRevD.86.079901, [Erratum: *Phys. Rev.* **D86**, 079901 (2012)].

135. Y.-M. Wang and Y.-L. Shen, *JHEP* **02**, 179 (2016), [arXiv:1511.09036 \[hep-ph\]](#), [doi:10.1007/JHEP02\(2016\)179](#).
136. A. L. Kagan and M. Neubert, *Phys. Lett.* **B539**, 227 (2002), [arXiv:hep-ph/0110078 \[hep-ph\]](#), [doi:10.1016/S0370-2693\(02\)02100-7](#).
137. M. Beneke, T. Feldmann and D. Seidel, *Nucl. Phys.* **B612**, 25 (2001), [arXiv:hep-ph/0106067 \[hep-ph\]](#), [doi:10.1016/S0550-3213\(01\)00366-2](#).
138. M. Dimou, J. Lyon and R. Zwicky, *Phys. Rev.* **D87**, 074008 (2013), [arXiv:1212.2242 \[hep-ph\]](#), [doi:10.1103/PhysRevD.87.074008](#).
139. C. Bobeth, M. Chrzaszcz, D. van Dyk and J. Virto (2017), [arXiv:1707.07305 \[hep-ph\]](#).
140. F. Kruger and L. M. Sehgal, *Phys. Lett.* **B380**, 199 (1996), [arXiv:hep-ph/9603237 \[hep-ph\]](#), [doi:10.1016/0370-2693\(96\)00413-3](#).
141. M. Beneke, T. Feldmann and D. Seidel, *Eur. Phys. J.* **C41**, 173 (2005), [arXiv:hep-ph/0412400 \[hep-ph\]](#), [doi:10.1140/epjc/s2005-02181-5](#).
142. A. Khodjamirian, T. Mannel, A. A. Pivovarov and Y. M. Wang, *JHEP* **09**, 089 (2010), [arXiv:1006.4945 \[hep-ph\]](#), [doi:10.1007/JHEP09\(2010\)089](#).
143. A. Khodjamirian, T. Mannel and Y. M. Wang, *JHEP* **02**, 010 (2013), [arXiv:1211.0234 \[hep-ph\]](#), [doi:10.1007/JHEP02\(2013\)010](#).
144. U. Egede, T. Hurth, J. Matias, M. Ramon and W. Reece, *JHEP* **11**, 032 (2008), [arXiv:0807.2589 \[hep-ph\]](#), [doi:10.1088/1126-6708/2008/11/032](#).
145. U. Egede, T. Hurth, J. Matias, M. Ramon and W. Reece, *JHEP* **10**, 056 (2010), [arXiv:1005.0571 \[hep-ph\]](#), [doi:10.1007/JHEP10\(2010\)056](#).
146. D. Becirevic and E. Schneider, *Nucl. Phys.* **B854**, 321 (2012), [arXiv:1106.3283 \[hep-ph\]](#), [doi:10.1016/j.nuclphysb.2011.09.004](#).
147. B. Grinstein and D. Pirjol, *Phys. Rev.* **D70**, 114005 (2004), [arXiv:hep-ph/0404250 \[hep-ph\]](#), [doi:10.1103/PhysRevD.70.114005](#).
148. C. Hambrock, G. Hiller, S. Schacht and R. Zwicky, *Phys. Rev.* **D89**, 074014 (2014), [arXiv:1308.4379 \[hep-ph\]](#), [doi:10.1103/PhysRevD.89.074014](#).
149. G. Hiller and R. Zwicky, *JHEP* **03**, 042 (2014), [arXiv:1312.1923 \[hep-ph\]](#), [doi:10.1007/JHEP03\(2014\)042](#).
150. J. Lyon and R. Zwicky (2014), [arXiv:1406.0566 \[hep-ph\]](#).
151. S. Braß, G. Hiller and I. Nisandzic, *Eur. Phys. J.* **C77**, 16 (2017), [arXiv:1606.00775 \[hep-ph\]](#), [doi:10.1140/epjc/s10052-016-4576-9](#).
152. T. Feldmann, B. Müller and D. Seidel, *JHEP* **08**, 105 (2017), [arXiv:1705.05891 \[hep-ph\]](#), [doi:10.1007/JHEP08\(2017\)105](#).
153. T. Hermann, M. Misiak and M. Steinhauser, *JHEP* **12**, 097 (2013), [arXiv:1311.1347 \[hep-ph\]](#), [doi:10.1007/JHEP12\(2013\)097](#).
154. K. De Bruyn, R. Fleischer, R. Knegjens, P. Koppenburg, M. Merk, A. Pellegrino and N. Tuning, *Phys. Rev. Lett.* **109**, 041801 (2012), [arXiv:1204.1737 \[hep-ph\]](#), [doi:10.1103/PhysRevLett.109.041801](#).
155. D. Straub, `flavio` - A Python package for flavour physics phenomenology in the Standard Model and beyond <https://flav-io.github.io>, (2018).
156. T. Hurth, C. Langenbruch and F. Mahmoudi, *JHEP* **11**, 176 (2017), [arXiv:1708.04474 \[hep-ph\]](#), [doi:10.1007/JHEP11\(2017\)176](#).
157. T. Blake, U. Egede, P. Owen, G. Pomery and K. A. Petridis (2017), [arXiv:1709.03921 \[hep-ph\]](#).
158. M. Chrzaszcz, A. Mauri, N. Serra, R. Silva Coutinho and D. van Dyk (2018), [arXiv:1805.06378 \[hep-ph\]](#).
159. A. Mauri, N. Serra and R. Silva Coutinho (2018), [arXiv:1805.06401 \[hep-ph\]](#).
160. F. Beaujean, C. Bobeth, D. van Dyk and C. Wacker, *JHEP* **08**, 030 (2012),

46 *Johannes Albrecht, Stefanie Reichert, Danny van Dyk*

- [arXiv:1205.1838](#) [[hep-ph](#)], doi:10.1007/JHEP08(2012)030.
161. M. Ciuchini, A. M. Coutinho, M. Fedele, E. Franco, A. Paul, L. Silvestrini and M. Valli, *Eur. Phys. J. C* **77**, 688 (2017), [arXiv:1704.05447](#) [[hep-ph](#)], doi:10.1140/epjc/s10052-017-5270-2.
162. T. Hurth, F. Mahmoudi, D. Martinez Santos and S. Neshatpour, *Phys. Rev.* **D96**, 095034 (2017), [arXiv:1705.06274](#) [[hep-ph](#)], doi:10.1103/PhysRevD.96.095034.
163. J. Albrecht, F. Bernlochner, M. Kenzie, S. Reichert, D. Straub and A. Tully (2017), [arXiv:1709.10308](#) [[hep-ph](#)].
164. LHCb Collaboration, (I. Bediaga *et al.*), Framework TDR for the LHCb Upgrade CERN-LHCC-2012-007, LHCb-TDR-12 <https://cds.cern.ch/record/1443882>, (2012).
165. 294th Meeting of Scientific Policy Committee, Medium-Term Plan for the period 2016-2020. CERN/SPC/1050, CERN/FC/5932, CERN/3197 <https://cds.cern.ch/record/2053977>, (2015).